

1 **Assessing Climate Change-Induced Flood Risk in the**
2 **Conasauga River Watershed: An Application of Ensemble**
3 **Hydrodynamic Inundation Modeling**

4
5 Tigstu T. Dullo¹, George K. Darkwah¹, Sudershan Gangrade^{2,3}, Mario Morales-
6 Hernández^{3,4}, Md Bulbul Sharif⁵, Alfred J. Kalyanapu^{1,*}, Shih-Chieh Kao^{2,3}, Sheikh
7 Ghafoor⁵, and Moetasim Ashfaq^{3,4}
8
9

10 ¹ Department of Civil and Environmental Engineering, Tennessee Technological
11 University, Cookeville, TN 38505, USA

12 ² Environmental Sciences Division, Oak Ridge National Laboratory, Oak Ridge, TN
13 37831, USA

14 ³ Climate Change Science Institute, Oak Ridge National Laboratory, Oak Ridge, TN
15 37831, USA

16 ⁴ Computational Sciences and Engineering Division, Oak Ridge National Laboratory,
17 Oak Ridge, TN 37831, USA

18 ⁵ Department of Computer Science, Tennessee Technological University, Cookeville, TN
19 38505, USA
20
21
22
23
24
25
26
27
28
29

30 *Corresponding Author

31 Alfred J. Kalyanapu, PhD

32 1020 Stadium Drive, P O Box 5015

33 Cookeville, TN 38505

34 Telephone: 931-372-3561

35 Email Address: akalyanapu@tntech.edu
36
37

38 Notice: This manuscript has been authored by UT-Battelle, LLC, under contract DE-AC05-
39 00OR22725 with the US Department of Energy (DOE). The US government retains and the
40 publisher, by accepting the article for publication, acknowledges that the US government retains a
41 nonexclusive, paid-up, irrevocable, worldwide license to publish or reproduce the published form
42 of this manuscript, or allow others to do so, for US government purposes. DOE will provide
43 public access to these results of federally sponsored research in accordance with the DOE Public
44 Access Plan (<http://energy.gov/downloads/doe-public-access-plan>).
45

46 **Abstract**

47 This study evaluates the impact of potential future climate change on flood regimes,
48 floodplain protection, and electricity infrastructures across the Conasauga River
49 Watershed in the southeastern United States through ensemble hydrodynamic inundation
50 modeling. The ensemble streamflow scenarios were simulated by the Distributed
51 Hydrology Soil Vegetation Model (DHSVM) driven by (1) 1981–2012 Daymet
52 meteorological observations, and (2) eleven sets of downscaled global climate models
53 (GCMs) during the 1966–2005 historical and 2011–2050 future periods. Surface
54 inundation was simulated using a GPU-accelerated Two-dimensional Runoff Inundation
55 Toolkit for Operational Needs (TRITON) hydrodynamic model. Nine out of the eleven
56 GCMs exhibit an increase in the mean ensemble flood inundation areas. Moreover, at the
57 1% annual exceedance probability level, the flood inundation frequency curves indicate a
58 ~16 km² increase in floodplain area. The assessment also shows that even after flood-
59 proofing, four of the substations could still be affected in the projected future period. The
60 increase in floodplain area and substation vulnerability highlights the need to account for
61 climate change in floodplain management. Overall, this study provides a proof-of-
62 concept demonstration of how the computationally intensive hydrodynamic inundation
63 modeling can be used to enhance flood frequency maps and vulnerability assessment
64 under the changing climatic conditions.

65

66 **Keywords:** Flood simulation; Climate change; Critical electricity infrastructure;
67 Floodplain protection standards.

68 **1. Introduction**

69 Floods are costly disasters that affect more people than any other natural hazard
70 around the world (UNISDR, 2015). Major factors that can exacerbate flood damage
71 include population growth, urbanization, and climate change (Birhanu et al., 2016;
72 Winsemius et al., 2016; Alfieri et al., 2017; Alfieri et al., 2018; Kefi et al., 2018). Recent
73 observations exhibit an increase in the frequency and the intensity of extreme
74 precipitation events (Pachauri and Meyer, 2014), which have strengthened the magnitude
75 and frequency of flooding (Milly et al., 2002; Langerwisch et al., 2013; Alfieri et al.,
76 2015a; Alfieri et al., 2018; Mora et al., 2018). As a result, the damage and cost of
77 flooding have substantially increased across the United States (US) (Pielke Jr. and
78 Downton, 2000; Pielke Jr. et al., 2002; Ntelekos et al., 2010; Wing et al., 2018) and the
79 rest of the world (Hirabayashi et al., 2013; Arnell and Gosling, 2014; Alfieri et al.,
80 2015b; Alfieri et al., 2017; Kefi et al., 2018).

81 Since 1968, the National Flood Insurance Program (NFIP), administered by the
82 Federal Emergency Management Agency (FEMA), has implemented floodplain
83 regulation standards in the US to mitigate the escalating flood losses (FEMA, 2002). For
84 communities participating in the NFIP, flood insurance is required for structures located
85 within the 1% annual exceedance probability (AEP) flood zone (i.e., areas with
86 probability of flooding $\geq 1\%$ in any given year; FEMA, 2002). However, existing
87 floodplain protection standards have proven to be inadequate (Galloway et al., 2006;
88 Ntelekos et al., 2010; Tan, 2013; Blessing et al., 2017; HCFCD, 2018), and climate
89 change can likely exacerbate these issues (Olsen, 2006; Ntelekos et al., 2010; Kollat et
90 al., 2012; AECOM, 2013; Wobus et al., 2017; Nyaupane et al., 2018; Pralle, 2019). For

91 instance, the streamflow AEP thresholds and synthetic hydrographs used to simulate the
92 flood zones were derived purely based on historic observations that may underestimate
93 the intensified hydrologic extremes in the projected future climatic conditions. Although
94 the possible change of future streamflow AEP thresholds may be evaluated by an
95 ensemble of hydrologic model outputs driven by multiple downscaled and bias-corrected
96 climate models (e.g., Wobus et al., 2017), the extension from maximum streamflow to
97 maximum flood zone is not trivial, and cannot be explicitly addressed through the
98 conventional deterministic inundation modeling approach.

99 The increases in the magnitude and frequency of flooding, in addition to the
100 inadequacy of floodplain measures and the high costs of hardening (Wilbanks et al.,
101 2008; Farber-DeAnda et al., 2010; Gilstrap et al., 2015), have put electricity
102 infrastructures at risk (Zamuda et al., 2015; Zamuda and Lippert, 2016; Cronin et al.,
103 2018; Forzieri et al., 2018; Mikellidou et al., 2018; Allen-Dumas et al., 2019). In
104 particular, electricity infrastructures which lie in areas vulnerable to flooding can
105 experience floodwater damages that may lead to changes in their energy production and
106 consumption (Chandramowli and Felder, 2014; Ciscar and Dowling, 2014; Bollinger and
107 Dijkema, 2016; Gangrade et al., 2019). For instance, flooding can rust metals, destroy
108 insulation, and damage interruption capacity (Farber-DeAnda et al., 2010; Vale, 2014;
109 NERC, 2018; Bragatto et al., 2019). It is estimated that nearly 300 energy facilities are
110 located on low-lying lands vulnerable to sea-level rise and flooding in the lower 48 US
111 states, (Strauss and Ziemiński, 2012).

112 Several studies have assessed the vulnerability of electricity infrastructures to
113 flooding (Reed et al., 2009; Winkler et al., 2010; Bollinger and Dijkema, 2016; Fu et al.,

114 2017; Pant et al., 2017; Bragatto et al., 2019; Gangrade et al., 2019). For highly sensitive
115 water infrastructures such as dams (McCuen, 2005), Gangrade et al. (2019) showed that
116 the surface inundation associated with probable maximum flood (PMF) is generally
117 projected to increase in future climate conditions. However, given the extremely large
118 magnitude of PMF (AEP < 10^{-4} %), the findings cannot be directly associated with more
119 frequent and moderate flood events (i.e., AEP around 1–0.2%) that are the main focus of
120 many engineering applications. Although some of these studies focused on evaluating the
121 resilience of electricity infrastructures against flood hazard and/or climate change, only a
122 few of them evaluated site-specific inundation risk and quantified impacts of climate
123 change-induced flooding on electricity infrastructures under different future climate
124 scenarios. Again, one main challenge is associated with the high computational costs to
125 effectively transform ensemble streamflow projections into ensemble surface inundation
126 projections through hydrodynamic models. With the enhanced inundation models and
127 high-performance computing (HPC) capabilities (Morales-Hernández et al., 2020), this
128 challenge can be gradually overcome for more spatially explicit flood vulnerability
129 assessment.

130 The objective of this study is to demonstrate the applicability of a computationally
131 intensive ensemble inundation modeling approach to better understand how climate
132 change may affect flood regimes, floodplain regulation standards, and the vulnerability of
133 existing infrastructures. Extending from the framework developed by Gangrade et al.
134 (2019) for PMF-scale events (AEP < 10^{-4} %) based on one selected climate model
135 (CCSM4), we focus on more frequent extreme streamflow events (i.e., AEP around 1–
136 0.2%) which requires different modeling strategies based on multiple downscaled climate

137 models. The unique aspects of this study are the application of an integrated climate-
138 hydrologic-hydraulic modeling framework for:

139 (1) Evaluating the changes in flood regime using high-resolution ensemble flood
140 inundation maps. The ensemble-based approach is able to incorporate the large
141 hydrologic interannual variability and model uncertainty that cannot be captured
142 through the conventional deterministic flood map.

143 (2) Enabling direct frequency analysis of ensemble flood inundation maps that
144 correspond to historic and projected future climate conditions. This approach
145 provides an alternative floodplain delineation technique to the conventional
146 approach, in which a single deterministic design flood value is used to develop a
147 flood map with a given exceedance probability.

148 (3) Evaluating the vulnerability of electricity infrastructures to climate change-
149 induced flooding and assessing the adequacy of existing flood protection
150 measures using ensemble flood inundation. This information will help floodplain
151 managers to identify the most vulnerable infrastructures and recommend suitable
152 adaptation measures.

153 The following technique was adopted in this study. First, we generated streamflow
154 projection by utilizing an ensemble of simulated streamflow hydrographs driven by both
155 historical observations and downscaled climate projections (Gangrade et al., 2020) as
156 inputs for hydrodynamic inundation modeling as presented in section 2.2. Then, we set
157 up and calibrated a 2D hydrodynamic inundation model, Two-dimensional Runoff
158 Inundation Toolkit for Operational Needs (TRITON; Morales-Hernández et al., 2021), in
159 our study area which is presented in section 2.3. For inundation modeling, sensitivity

160 analyses were conducted on three selected parameters to quantify and compare their
161 respective influences on modeled flood depths and extents. The performance of TRITON
162 was then evaluated by comparing a simulated 1% AEP flood map with the reference 1%
163 AEP flood map from the Federal Emergency Management Agency (FEMA). Finally, as
164 presented in sections 2.4 and 2.5, ensemble inundation modeling was performed to
165 develop flood inundation frequency curves and maps, and to assess the vulnerability of
166 electricity infrastructures under a changing climate, respectively.

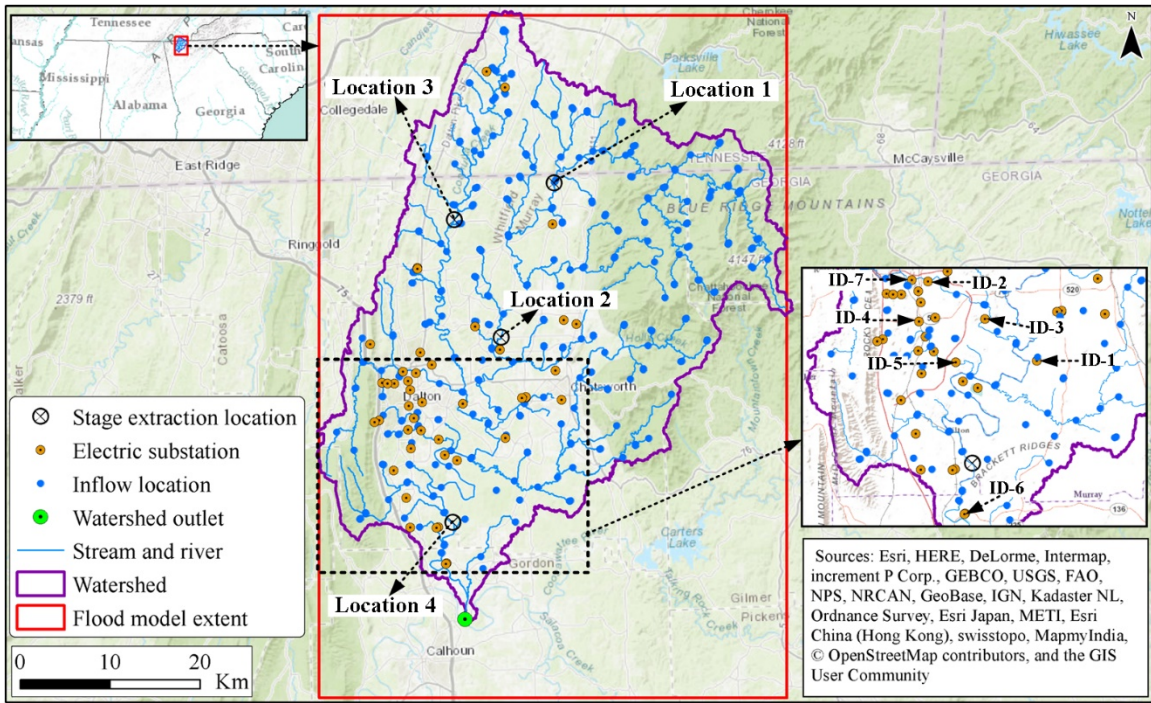
167 The article is organized as follows: the data and methods are discussed in Section 2;
168 Section 3 presents the result and discussion; and the summary is presented in Section 4.

169 **2. Data and Methods**

170 **2.1. Study Area**

171 Our study area is the Conasauga River Watershed (CRW) located in southeastern
172 Tennessee and northwestern Georgia (Figure 1). The CRW is an eight-digit Hydrologic
173 Unit Code (HUC08) subbasin (03150101) with a total drainage area of ~1880 km². The
174 northeastern portions of the watershed are rugged, mountainous areas largely covered
175 with forests (Ivey and Evans, 2000; Elliott and Vose, 2005). The CRW, which is one
176 headwater basin of the Alabama-Coosa-Tallapoosa (ACT) River Basin, rises high on the
177 Blue Ridge Mountains of Georgia and Tennessee and flows for 145 km before joining the
178 Coosawattee River to form the Oostanaula River (Ivey and Evans, 2000; USACE, 2013).
179 The CRW climate is characterized by warm, humid summers, and mild winters with
180 mean annual temperature of 15 to 20 °C and average annual precipitation of 1300 to 1400
181 mm (FIS, 2007; FIS, 2010; Baechler et al., 2015). The watershed encompasses four

182 counties: Bradley, Polk, Fannin, Murray, and Whitfield. It also includes the cities of
183 Dalton and Chatsworth, Georgia. There is no major reservoir located in the CRW.



184

185 Figure 1. Conasauga River Watershed study area location, model extent, electric
186 substations, and inflow locations. Background layer source: © OpenStreetMap
187 contributors 2020. Distributed under a Creative Commons BY-SA License.

188

189 2.2. Streamflow Projections

190 The ensemble streamflow projections were generated by a hierarchical modeling
191 framework, which started with regional climate downscaling followed by hydrologic
192 modeling (Gangrade et al., 2020). The climate projections were generated by dynamically
193 downscaling of 11 GCMs from the Coupled Model Intercomparison Project Phase-5
194 (CMIP5) data archive. Each GCM was used as lateral and lower boundary forcing in a
195 regional climate model RegCM4 (Giorgi et al., 2012) at a horizontal grid spacing of 18

196 km over a domain that covered continental US and parts of Canada and Mexico (Ashfaq
 197 et al., 2016) (Table 1). Each RegCM4 integration covered 40 years in the historic period
 198 (1966–2005; hereafter baseline) and another 40 years in the future period (2011–2050)
 199 under Representative Concentration Pathway 8.5 (RCP 8.5) emission scenario, with a
 200 combined 880 years of data across all RegCM4 simulations. To capture the multi-decadal
 201 climate variability, a minimum of 30-year period has been used in many studies (e.g.,
 202 Alfieri et al., 2015a, 2015b). Given the additional data available from Gangrade et al.
 203 (2020), we have adopted a longer 40-year period that may further enlarge the sample
 204 space to better support the statistical analyses in this study.

205
 206 Table 1. Summary of the 11 dynamically downscaled climate models (adopted from
 207 Ashfaq et al., 2016).

S. No.	Climate model name	Number of flood events per climate model	Time period	
1	ACCESS1-0			
2	BCC-CSM1-1			
3	CCSM4			
4	CMCC-CM			
5	FGOALS-g2		1966–2005	2011-2050
6	GFDL-ESM2M	40	(Baseline)	(Future/RCP
7	MIROC5			8.5)
8	MPI-ESM-MR			
9	MRI-CGCM3			
10	NorESM1-M			
11	IPSL-CM5A-LR			

208

209 The RegCM4 simulated daily precipitation and temperature were further statistically
210 bias-corrected to a spatial resolution of 4 km following a quantile mapping technique,
211 described in Ashfaq et al. (2010, 2013). The 4 km Parameter-elevation Regressions on
212 Independent Slopes Model (PRISM; Daly et al., 2008) data was used as the historic
213 observations to support bias-correction. In the baseline period, the simulated quantiles of
214 precipitation and temperature were corrected by mapping them onto the observed
215 quantiles. In the future period, the monthly quantile shifts were calculated based on the
216 simulated baseline and future quantiles which were subsequently added to the bias
217 corrected baseline quantiles to generate bias-corrected monthly future data. Finally, the
218 monthly bias-corrections were distributed to the daily values while preserving in each
219 time period. This approach substantially improves the biases in the modeled daily
220 precipitation and temperature while preserving the simulated climate change signal.
221 Further details of the bias-correction are provided in Ashfaq et al. (2010, 2013) while the
222 information regarding the RegCM4 configuration, evaluation and future climate
223 projections are detailed in Ashfaq et al. (2016).

224 The hydrologic simulations were then conducted using the Distributed Hydrology
225 Soil Vegetation Model (DHSVM; Wigmosta et al., 1994), which is a process-based high-
226 resolution hydrologic model that can capture heterogeneous watershed processes and
227 meteorology at a fine resolution. DHSVM uses spatially distributed parameters, including
228 topography, soil types, soil depths, and vegetation types. The input meteorological data
229 includes precipitation, incoming shortwave and longwave radiation, relative humidity, air
230 temperature and wind speed (Wigmosta et al., 1994; Storck et al., 1998; Wigmosta et al.,
231 2002). The DHSVM performance and applicability has been reported in various earlier

232 climate and flood related studies (Elsner et al., 2010; Hou et al., 2019; Gangrade et al.,
233 2018, 2019, 2020). A calibrated DHSVM implementation from Gangrade et al. (2018) at
234 90 m grid spacing was used to produce 3-hourly streamflow projections using the
235 RegCM4 meteorological forcings described in the previous section (Table 1). In addition,
236 a control simulation driven by 1981–2012 Daymet meteorologic forcings (Thornton et
237 al., 1997) was conducted for model evaluation and validation. The hydrologic simulations
238 used in this study are a part of a larger hydroclimate assessment effort for the ACT River
239 Basin, as detailed in Gangrade et al. (2020). Since there is no major reservoir in the
240 CRW, the additional reservoir operation module (Zhao et al., 2016) was not needed in
241 this study.

242 Note that while the ensemble streamflow projections based on dynamical
243 downscaling and high-resolution hydrologic modeling from Gangrade et al. (2020) are
244 suitable to explore extreme hydrologic events in this study, they do not represent the full
245 range of possible future scenarios. Additional factors such as other GCMs, RCP
246 scenarios, downscaling approaches, and hydrologic models and parameterization may
247 also affect future streamflow projections. In other words, although these ensemble
248 streamflow projections can tell us how likely the future streamflow magnitude may
249 change from the baseline level, they are not the absolute prediction into the future. In
250 practice, these modeling choices will likely be study-specific based on the agreement
251 among key stakeholders. It is also noted that the new Coupled Model Intercomparison
252 Project Phase-6 (CMIP6) data have also become available to update the ensemble
253 streamflow projections, but is not pursued in this study.

254 **2.3. Inundation Modeling**

255 The ensemble inundation modeling was performed using TRITON, which is a
256 computationally enhanced version of Flood2D-GPU (Kalyanapu et al., 2011). TRITON
257 allows parallel computing using multiple graphics processing units (GPUs) through a
258 hybrid Message Passing Interface (MPI) and Compute Unified Device Architecture
259 (CUDA) (Morales-Hernández et al., 2021). TRITON solves the nonlinear hyperbolic
260 shallow water equations using an explicit upwind finite-volume scheme, based on Roe's
261 linearization. The shallow water equations are a simplified version of the Navier-Stokes
262 equations in which the horizontal momentum and continuity equations are integrated in
263 the vertical direction (see Morales-Hernández et al., (2021), for further model details). An
264 evaluation of TRITON performance for the CRW is presented and discussed in Section
265 3.3.

266 TRITON's input data includes digital elevation model (DEM), surface roughness,
267 initial depths, flow hydrographs, and inflow source locations (Kalyanapu et al., 2011;
268 Marshall et al., 2018; Morales-Hernández et al., 2020; Morales-Hernández et al., 2021).
269 In this study, the hydraulic and geometric parameters from the flood model evaluation
270 section (Section 3.3) were used in the flood simulation. The topography was represented
271 using the one-third arc-second (~10 m) spatial resolution DEM (Archuleta et al., 2017)
272 from the US Geological Survey (USGS). To improve the quality of the base DEM, as
273 discussed in the flood model evaluation section, the main channel elevation was reduced
274 by 0.15 m. Elevated roads and bridges that obstruct the flow of water were also removed.
275 For surface roughness, we used a single channel Manning's n value of 0.05 and a single
276 floodplain Manning's n value of 0.35. The selection of channel and floodplain Manning's
277 n value was based on the Whitfield County Flood Insurance Study (FIS, 2007), which

278 reported a range of Manning's n values estimated from field observations and
279 engineering judgment for about 15 streams inside the CRW (section 3.2). Furthermore, a
280 water depth value of 0.35 m was defined for the main river channel as an initial boundary
281 condition. The zero velocity gradients were used as the downstream boundary condition.
282 Further discussion of model parameter sensitivity and model evaluation are provided in
283 sections 3.2 and 3.3.

284 The simulated DHSVM streamflow was used to prepare inflow hydrographs for
285 ensemble inundation modeling. To provide a large sample size for frequency analysis, we
286 selected all annual maximum peak streamflow events (the maximum corresponded to the
287 outlet of CRW [Figure 1]) from the 1981–2012 control simulation (32 years), the 1966–
288 2005 baseline simulation (440 years; 40 years \times 11 models), and the 2011–2050 future
289 simulation (440 years; 40 years \times 11 models), with a total of 912 events. For each annual
290 maximum event, the 3-hour timestep, 10-day hydrographs (which capture the peak CRW
291 outlet discharge) across all DHSVM river segments were summarized. Following a
292 procedure similar to Gangrade et al. (2019), these streamflow hydrographs were
293 converted to TRITON inputs at 300 inflow locations selected along the NHD+ river
294 network in the CRW (Figure 1). The TRITON model extent, shown in Figure 1, has an
295 approximate area of 3945 km² and includes ~44 million model grid cells (7976 rows \times
296 5474 columns in a uniform structured mesh). The ensemble flood simulations resulted in
297 gridded flood depth and velocity output at 30-minute intervals. The simulations generated
298 an approximately 400 Terabyte data and utilized ~2000 node hours on the Summit
299 supercomputer, managed by the Oak Ridge Leadership Computing Facility at Oak Ridge
300 National Laboratory.

301 **2.4. Flood Inundation Frequency Analysis**

302 Given the nature of GCM experiments, each set of climate projections can be
303 considered as a physics-based realization of historic and future climate under specified
304 emission scenarios. Therefore, an ensemble of multimodel simulations can effectively
305 increase the data lengths and sample sizes that are keys to support frequency analysis,
306 especially for low-AEP events. In this study, we conducted flood frequency analyses
307 separately for the 1966–2005 baseline and 2011–2050 future periods so that the
308 difference between the two periods represent the changes in flood risk due to climate
309 change.

310 To prepare the flood frequency analysis, we first calculated the maximum flood depth
311 at every grid in each simulation. A minimum threshold of 10 cm flood depth was used to
312 judge whether a cell was wet or dry (Gangrade et al., 2019). Further, for a given grid cell,
313 if the total number of non-zero flood depth values (i.e., of the 440 depth values) was less
314 than 30, the grid cell was also considered dry. This threshold was selected based on the
315 minimum sample size requirement for flood depth frequency analysis suggested by Li et
316 al. (2018). Next, we calculated the maximum flooded area (hereafter used alternatively
317 with “floodplain area”) for each simulation. A log-Pearson Type III (LP3) distribution
318 was then used for frequency analysis following the guidelines outlined in Bulletins 17B
319 (USGS, 1982; Burkey, 2009) and 17C (England Jr. et al., 2019). Two types of LP3 fitting
320 were performed. The first type of fitting is event-based that fitted LP3 on the maximum
321 inundation area across all ensemble members. The second type of fitting is grid-based
322 (more computationally intensive) that fitted LP3 on the maximum flood depth at each
323 grid cell across all ensemble members. For both types of fittings, the frequency estimates

324 at 4%, 2%, 1%, and 0.5% AEP (corresponding to 25-, 50-, 100-, and 200-year return
325 levels) were derived for further analysis.

326 It is also noted that in addition to the annual maximum event approach used in this
327 study, one may also use the peak-over-threshold (POT) approach which can select
328 multiple streamflow events in a very wet year. While such an approach can lead to higher
329 extreme streamflow and inundation estimates, the timing of POT samples is fully
330 governed by the occurrences of wet years. In other words, if the trend of extreme
331 streamflow is significant in the future period, the POT samples will likely occur more in
332 the far future period. We hence select the annual maximum event approach that can
333 sample maximum streamflow events more evenly in time, which can better capture the
334 evolution of extreme events with time under the influence of climate change.

335 **2.5. Vulnerability of Electricity Infrastructure**

336 The vulnerability of electricity infrastructures to climate change-induced flooding
337 was evaluated using the ensemble flood inundation results. The 44 electric substations
338 (Figure 1) collected from the publicly available Homeland Infrastructure Foundation-
339 Level Data (HIFLD, 2019) were considered to be the electrical components susceptible to
340 flooding. To evaluate the vulnerability of these substations, we overlapped the maximum
341 flood extent from each ensemble member with all substations to identify the substations
342 that might be inundated under the baseline and future climate conditions. Further, as an
343 additional flood hazard indicator, the duration of inundation was estimated at each of the
344 affected substations using the ensemble flood simulation results.

345 The vulnerability analysis was performed for two different flood mitigation scenarios.
346 In the first scenario, we assumed that no flood protection measures were provided at all

347 substations. Hence, the substations that intersected with the flood footprint were
348 considered to be failed. In the second scenario, it was assumed that flood protection
349 measures were adopted for all substations following the FEMA P-1019 recommendation
350 (FEMA, 2014). According to FEMA P-1019 (FEMA, 2014), for emergency power
351 systems within critical facilities, the highest elevation among (1) the base flood elevation
352 (BFE: 1% FEMA AEP flood elevation) plus 3 feet (~0.91 m), (2) the locally adopted
353 design flood elevation, and (3) the 500-year flood elevation can be used to design flood
354 protection measures. Since the three recommended elevations were not available at all
355 substation locations, we focused only on the BFE plus ~0.91 m option. In addition, since
356 in the CRW the majority of existing flood insurance maps were classified as Zone A—
357 meaning that the special flood hazard areas were determined by approximate methods
358 without BFE values (FEMA, 2002)—we used the maximum flood depth values across all
359 control simulation years as the BFE values in this second mitigation scenario.

360 During the vulnerability analysis, we also assumed that (1) the one-third arc-second
361 spatial resolution DEM might reasonably represent the elevation of substations, (2)
362 existing substations would remain functional and would not be relocated, and (3) no
363 additional hardening measures (i.e., protections such as levees, berms, anchors, and
364 housings) will be adopted in the future period. Also, the cascading failure of a substation
365 due to grid interconnection was not considered in this study.

366

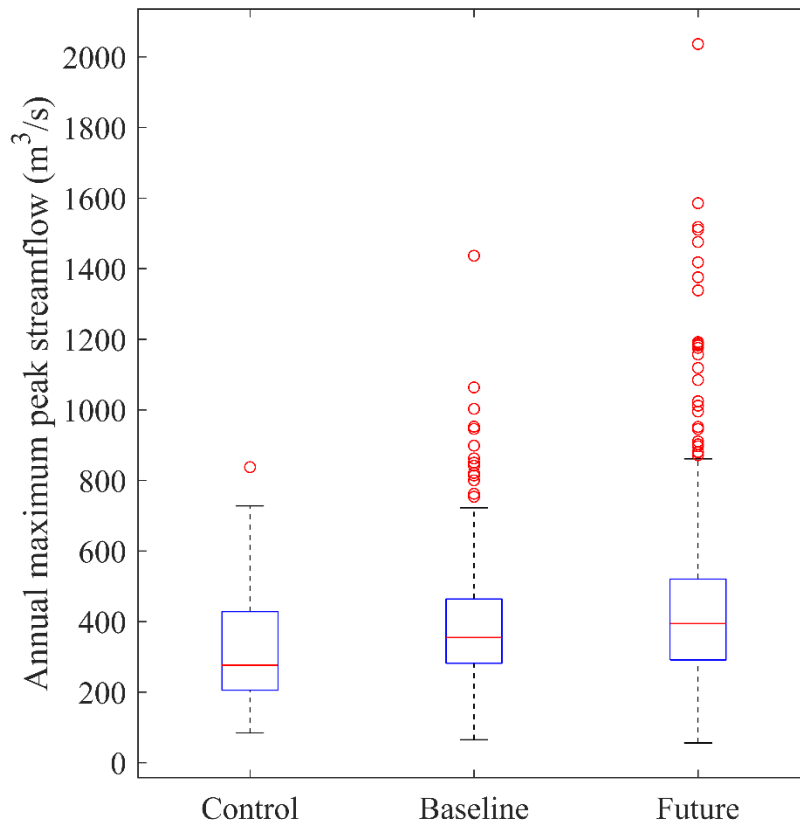
367 **3. Results and Discussion**

368 **3.1. Streamflow Projections**

369 This section presents a comparison of the annual maximum peak streamflow (at the
370 outlet of CRW) used in the control, baseline, and future simulations. The sample size
371 included 32 events from the control (1981–2012) simulation, 440 events from the
372 baseline (1966–2005) simulations, and another 440 events from the future (2011–2050)
373 simulations. These samples are illustrated in box and whisker plots in Figure 2, where
374 central mark indicate the median, while bottom and top edges indicate the 25th and 75th
375 percentiles respectively. The whiskers extend to the furthest data points not considered
376 outliers, which correspond to approximately ± 2.7 standard deviations and 99.3%
377 coverage if the data are normally distributed. As is evident from Figure 2, the
378 distributions of annual maximum peak streamflow values in the control and baseline
379 simulations are comparable. The upper and lower whiskers in the control simulation are
380 727.6 m³/s and 84.2 m³/s, which compare well to the 722.5 m³/s and 65.2 m³/s values in
381 the baseline simulation. In addition, we also conducted a two-tailed two-sample t-test (α
382 = 0.05) to compare if the means of control and baseline annual maximum streamflow are
383 statistically different. The results yielded a p-value of 0.09 which suggested that there is
384 no significant difference between the means of both control and baseline simulations. A
385 larger number of outliers are present in the baseline simulation, which is due to the larger
386 sample size (440 versus 32).

387 Under the future projection, an increase in the maximum peak streamflow is shown,
388 where the upper whisker in the future projection is ~21% higher than the baseline.
389 Moreover, the maximum of distribution in the future climate (2036.7 m³/s) is also much
390 higher than that in the baseline climate (1436.7 m³/s), suggesting a higher future flood

391 risk in the CRW. The increasing trend of streamflow extremes in the CRW is consistent
392 with the overall findings in the ACT River Basin (Gangrade et al., 2020).



393
394 Figure 2. A comparison of annual maximum peak streamflow at the outlet of Conasauga
395 River Watershed. The sample size includes 32 events from the control (1981–2012), 440
396 from the baseline (1966–2005), and another 440 from the future (2011–2050) periods.

397 3.2. Sensitivity Analysis for Flood Model

398 For a better understanding and selection of suitable TRITON parameters, a series of
399 sensitivity analyses were conducted using different combinations of Manning’s
400 roughness, initial water depths, and river bathymetry correction factors (Table 2).

401

402

403

404 Table 2. Summary of hydraulic and geometric parameters used in the sensitivity analysis.

Sensitivity parameter	Scenario	Initial water depth values (m)	Surface roughness (Manning's n values)	Bathymetry correction factor (m)
Initial water depth	1	0.00		
	2	0.15		
	3	0.35	$n_{ch} = 0.050 / n_{fldpl} = 0.350$	-0.15
	4	0.45		
	5	0.55		
	6	0.65		
Surface roughness	1		N_1: $n_{ch} = 0.035 / n_{fldpl} = 0.06$	
	2		N_2: $n_{ch} = 0.040 / n_{fldpl} = 0.25$	
	3		N_3: $n_{ch} = 0.045 / n_{fldpl} = 0.30$	
	4	0.35	N_4: $n_{ch} = 0.050 / n_{fldpl} = 0.35$	-0.15
	5		N_5: $n_{ch} = 0.055 / n_{fldpl} = 0.45$	
			N_6: $n_{ch} = 0.060 / n_{fldpl} = 0.50$	
	6		N_7: Manning's n map prepared based on the NLCD 2011	
Bathymetry correction factor	1			0.00
	2			-0.15
	3			-0.45
	4	0.35	$n_{ch} = 0.050 / n_{fldpl} = 0.350$	-0.75
	5			-1.00
	6			-1.25

405 Note: n_{ch} represents the Manning's n value in the main channel and n_{fldpl} represents the
 406 Manning's n value in the floodplain areas.

407

408 In calibrating a hydraulic model, it is a common practice to adjust the estimated
 409 Manning's n value, as it is the most uncertain and variable input hydraulic parameter
 410 (Brunner et al., 2016). In this study, we tested six different scenarios (Table 2) based on
 411 the Whitfield County Flood Insurance Study (FIS, 2007), which reported a range of
 412 Manning's n values estimated from field observations and engineering judgment for
 413 about 15 streams inside the CRW. It is noted that the depth variation of Manning's

414 roughness is not considered in the current study. Readers are referred to studies such as
415 Saksena et al. (2020) for additional information on the dynamic Manning's roughness for
416 potential hydrology and hydraulics applications.

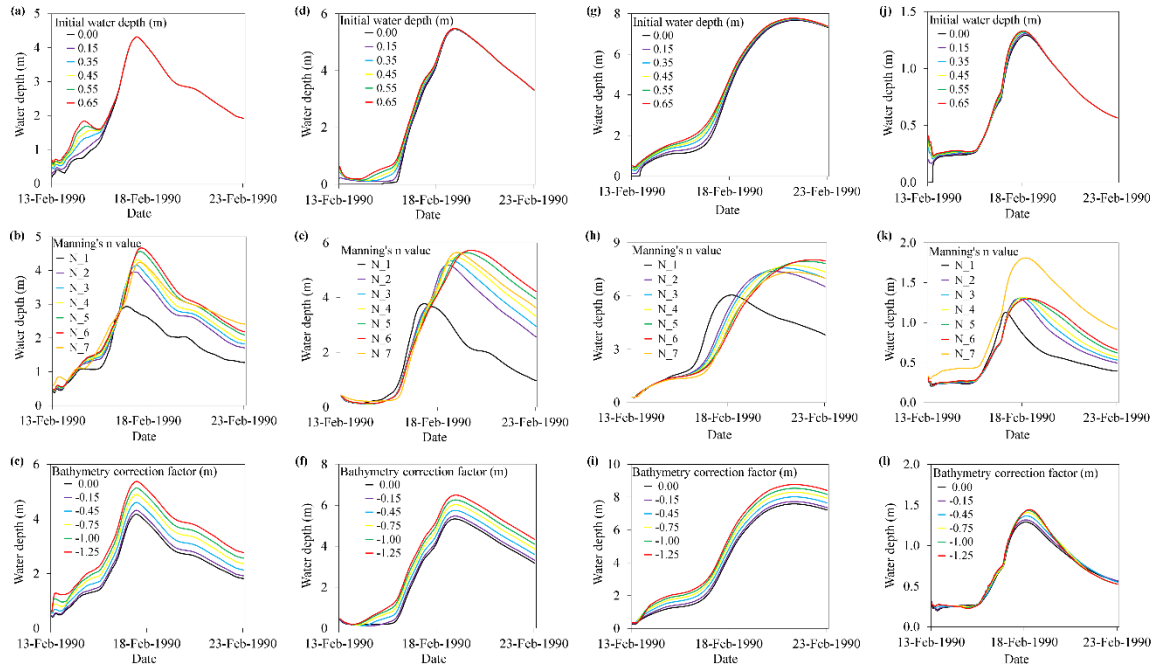
417 To establish an initial condition for TRITON, a sensitivity analysis was performed on
418 selected initial water depth values (ranging from 0 m to 0.65 m, Table 2) to understand
419 their relative effects. To select ranges for the initial water depth, we summarized the
420 observed water depth values that corresponds to low flow values at five USGS gauge
421 stations inside the CRW. The distribution of observed water depth values from the five
422 gauges showed average values ranging from 0.25 to 0.65m. Existing DEM products, even
423 those with high spatial resolution (i.e., 10 m or finer), do not represent the elevation of
424 river bathymetry accurately (Bhuyian et al., 2014). For the CRW, Bhuyian et al. (2019)
425 found that the one-third arc-second spatial resolution base DEM over-predicted the
426 inundation extent because of the bathymetric error, which reduced the channel
427 conveyance. In this study, we tested various bathymetry correction factors (ranging from
428 -1.25 m to 0 m, Table 2) by reducing the DEM elevation along the main channel to
429 understand the sensitivity of TRITON.

430 The sensitivity analysis was performed using the February 13–22, 1990 flood event
431 that has the maximum discharge among all 32 control simulation events. To evaluate
432 relative sensitivity of TRITON, we extracted simulated flood depths at four arbitrary
433 selected locations (Figure 1) and estimated the relative inundation area differences. The
434 impacts of initial water depths were significant only at the beginning where low flow
435 values dominated the hydrographs (Figure 3a, 3d, 3g, and 3j). Larger initial water depth
436 values generated higher flood inundation depths for both sample locations. Although the

437 differences in flood inundation extents relative to the dry bed show an increasing trend,
438 the relative differences are less than 1.4% (Figure 4a). Similarly, the differences in
439 average peak water depths and time to peak relative to the 0.35 m initial water depth were
440 less than 1.0% (Table 3). Increase in the channel and floodplain Manning's n values
441 resulted in higher flood depths for both sample locations (Figure 3b, 3e, 3h, and 3k). The
442 relative flood inundation area differences increase from about 23% to 31% (Figure 4b)
443 when the channel and floodplain Manning's n values are increased from 0.035 to 0.06
444 and from 0.06 to 0.50, respectively. In terms of simulated maximum flood extent, the
445 relative difference between scenario 3 (N_3) and scenario 7 (i.e., Manning's n map based
446 on different land use types [N_7]) showed ~16% (22 km²) change in inundation area
447 (Figure 4b). Similarly, the last scenario (N_7) resulted in ~9% increase in the average
448 peak water depth (Table 3), when compared to scenario 3 (N_3). Reduction in the
449 elevation of river bathymetry (to improve the quality of the base DEM) results in a direct
450 increase in maximum flood depth due to change in the river conveyance (Figure 3c, 3f,
451 3i, and 3l; Table 3). It also results in a decrease in the maximum flood extent (Figure 4c),
452 as more water is allowed to transport through the main channel instead of the floodplain.
453 Overall, the results showed that TRITON was more sensitive to the Manning's n values
454 than the initial water depths and bathymetric correction factors.

455

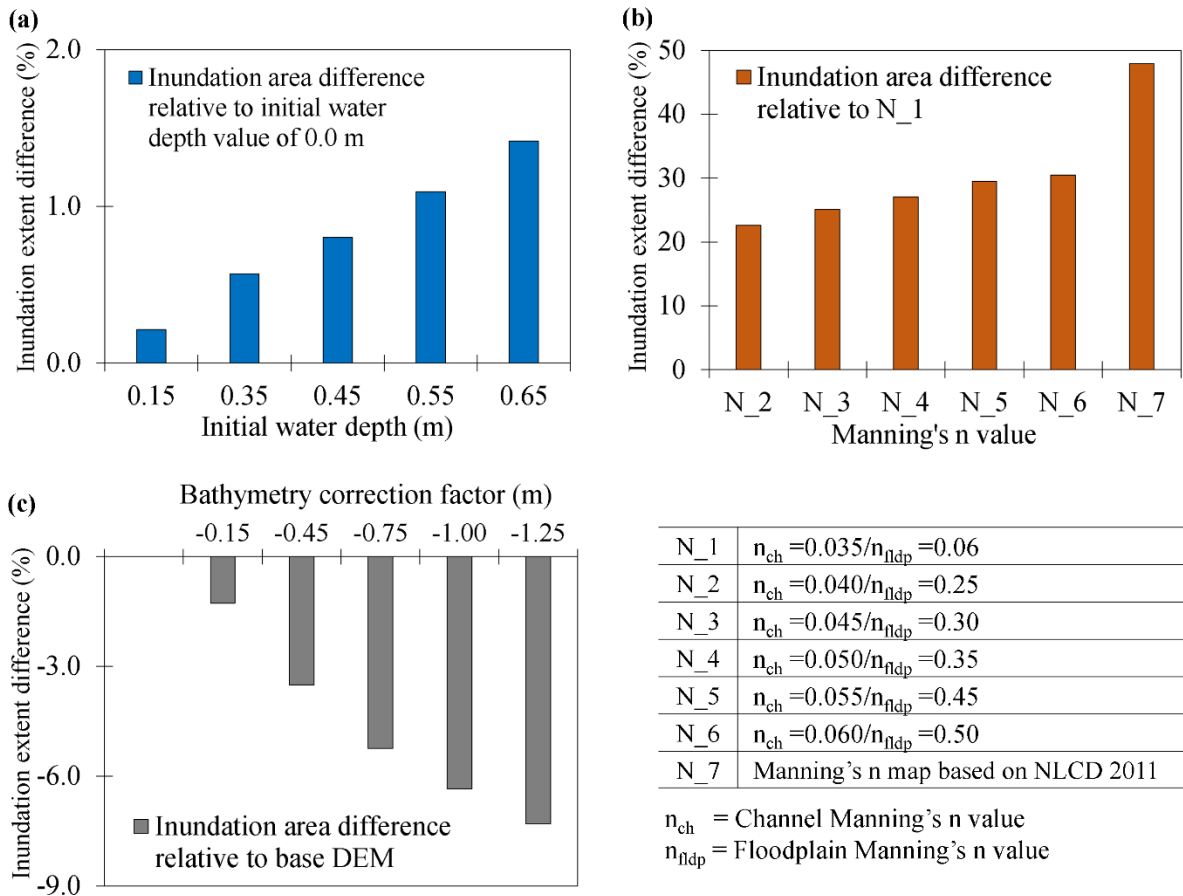
456



457

458 Figure 3. Simulated flood inundation depths extracted at location 1 (a, b, c) and
 459 location 2 (d, e, f). Note: Location 1 and 2 are shown in Figure 1. A description of the
 460 Manning's n values (N_1 to N_6) can be found in Table 2.

461



462

463 Figure 4. Change in simulated maximum flood inundation extents for (a) initial water
 464 depth, (b) Manning's n value, and (c) bathymetry correction factor.

465

466 Table 3. Change in peak water depth and time to peak.

Sensitivity parameter		% change in peak water depth	% change in time to peak	Scenarios used to calculate the % change values
Initial water depth (m)	0.00	-0.77	0.59	0.35 m water depth
	0.15	-0.41	0.25	
	0.35	0.00	0.00	
	0.45	0.16	-0.17	
	0.55	0.29	-0.33	
	0.65	0.42	-0.43	
N_1: $n_{ch} = 0.035 / n_{fldp} = 0.06$		-24.80	-24.53	N_4

Manning's n value	N_2: nch =0.040 / nfldpl =0.25	-4.79	-7.44	
	N_3: nch =0.045 / nfldpl =0.30	-2.11	-3.03	
	N_4: nch =0.050 / nfldpl =0.35	0.00	0.00	
	N_5: nch =0.055 / nfldpl =0.45	2.54	5.74	
	N_6: nch =0.060 / nfldpl =0.50	3.83	8.88	
	N_7: Manning's n map prepared based on the NLCD 2011	8.50	1.31	
	Bathymetry correction factor (m)	0.00 -0.15 -0.45 -0.75 -1.00 -1.25	-2.44 0.00 4.78 9.41 13.11 16.58	-0.10 0.00 0.19 0.50 0.86 1.17

467

468

469 3.3. Flood Model Evaluation

470 Because of a lack of observed streamflow data in the CRW, the performance of
471 TRITON was evaluated by comparing the simulated 1% AEP flood map with the
472 published 1% AEP flood map from FEMA (FEMA, 2019). The purpose of this
473 assessment is to understand whether TRITON can provide comparable results to the
474 widely accepted FEMA flood estimates. While the FEMA AEP flood maps do not
475 necessarily represent complete ground truth, such a comparison is the best option given
476 the data challenge. Similar approach has been utilized by several previous studies in the
477 evaluation of large-scale flood inundation evaluation (Alfieri et al., 2014; Wing et al.,
478 2017; Zheng et al., 2018; Gangrade et al., 2019).

479 To derive the 1% AEP flood map using TRITON, the ensemble-based approach used
480 by Gangrade et al. (2019) was followed. The assessment started by preparing the
481 streamflow hydrographs used to construct the 1% AEP flood map. The 1981–2012
482 annual maximum peak events and their corresponding 10-day streamflow hydrographs
483 were extracted from the control simulation. These streamflow hydrographs were then

484 proportionally rescaled to match the 1% AEP peak discharge estimated at the watershed
485 outlet (Figure 1), following the frequency analysis procedures outlined in Bulletin 17C
486 (England Jr. et al., 2019). The streamflow hydrographs from control simulations were
487 used for the peak discharge frequency analysis.

488 The results reported in the sensitivity analysis were also used to help identify suitable
489 TRITON parameters. In addition to streamflow hydrographs, TRITON requires DEM,
490 initial water depth, and Manning's n value. To minimize the effect of bathymetric error in
491 the base DEM (Bhuyian et al., 2014; Bhuyian et al., 2019), we reduced the elevation
492 along the main channel by 0.15 m (i.e., a bathymetry correction factor). Although this
493 simple approach is unlikely to adjust the channel bathymetry to its true values, it can
494 improve the channel conveyance volume that is lost in the base DEM. To further improve
495 the quality of the base DEM, we removed elevated roads and bridges that could obstruct
496 the flow of water in some of the streams and rivers. An initial water depth of 0.35 m was
497 also selected in this study. For the surface roughness, a couple of flood simulations were
498 performed by adjusting the Manning's n values for the main channel and floodplain to
499 achieve satisfactory agreement between the simulated and the reference FEMA flood
500 map. We eventually selected a single channel Manning's n value of 0.05 and a single
501 floodplain Manning's n value of 0.35.

502 Three evaluation metrics, including fit, omission, and commission (Kalyanapu et al.,
503 2011) were used to quantify the differences between the modeled and reference flood
504 map. The measure of fit determines the degree of relationship, while the omission and
505 commission statistically compare the simulated and reference FEMA flood maps
506 (Kalyanapu et al., 2011). The comparison between the simulated maximum inundation

507 and the corresponding 1% AEP FEMA flood map showed 80.65% fit, 5.52%
508 commission, and 15.36% omission (Figure 5), demonstrating that the TRITON could
509 reasonably estimate flood inundation extent, and depths in the CRW. The computational
510 efficiency of TRITON can further support ensemble inundation modeling to provide
511 additional variability information that cannot be provided by the conventional
512 deterministic flood map.

513 Although we have obtained satisfactory model performance for the purpose of our
514 study, the flood model implementation has some limitations that may be enhanced in
515 future studies. They include:

- 516 • Spatially varying Manning's n values may be derived based on high-resolution
517 land use land cover (LULC) conditions to better represent the spatial
518 heterogeneity in the modeling domain.
- 519 • Apart from changes in future runoff and streamflow, projections of future LULC
520 and its corresponding surface roughness can be considered to understand the
521 broader impacts due to environment change.
- 522 • In this study, we corrected DEM bias along the river channel cells by simplified
523 bathymetry correction factors. More sophisticated bathymetric configuration (i.e.,
524 channel shape and sinuosity) can be considered to better represent channel
525 conveyance.
- 526 • The current TRITON model does not provide capability to route local runoff and
527 external inflows through stormwater drainage systems. Coupling with additional
528 stormwater drainage models can be a potential future direction.

529 • Hydraulic and civil structures such as bridges, culverts, and weirs have not been
530 included since TRITON does not provide for the modeling of such components.
531 This can affect the accuracy of the flood depths, velocities, and flood extents
532 around these structures.
533

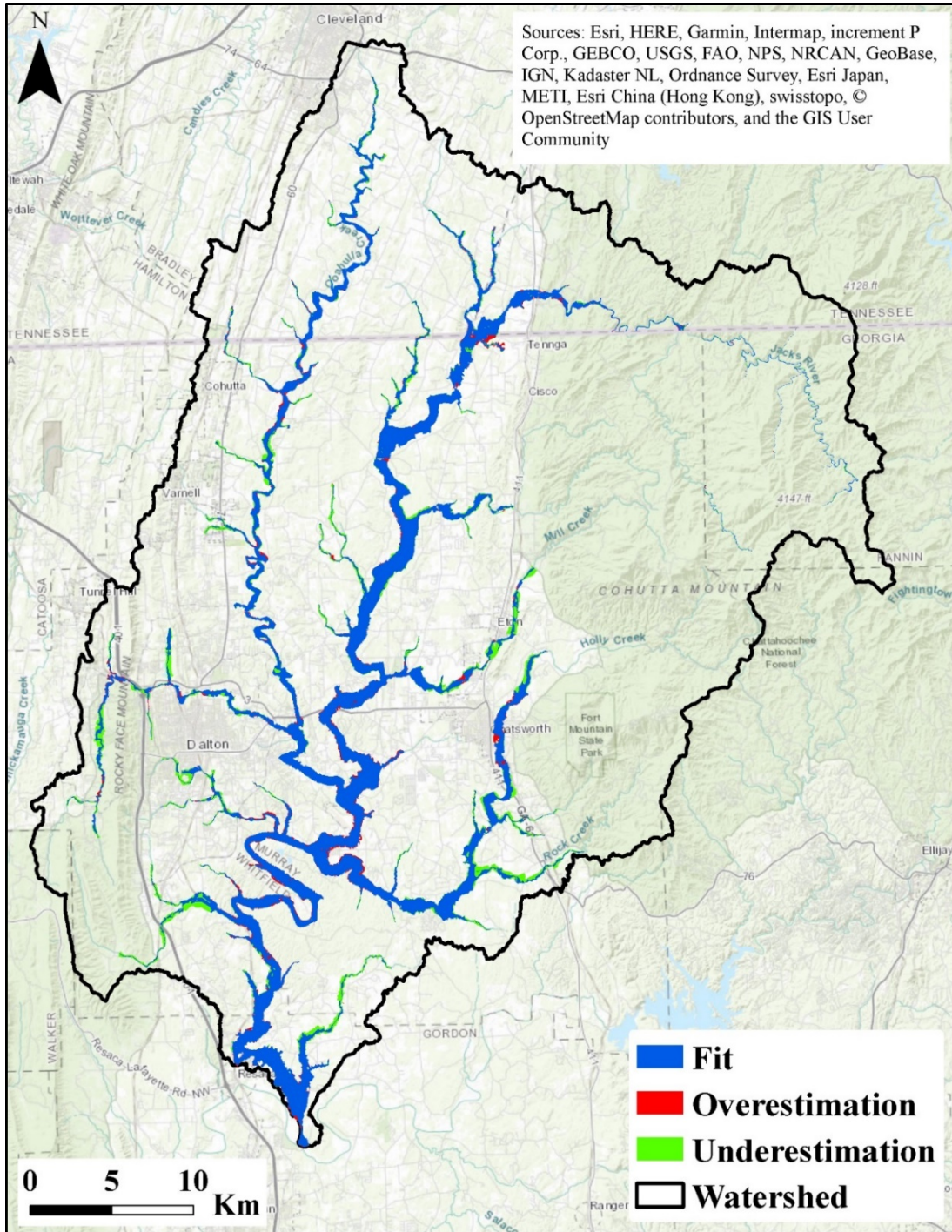


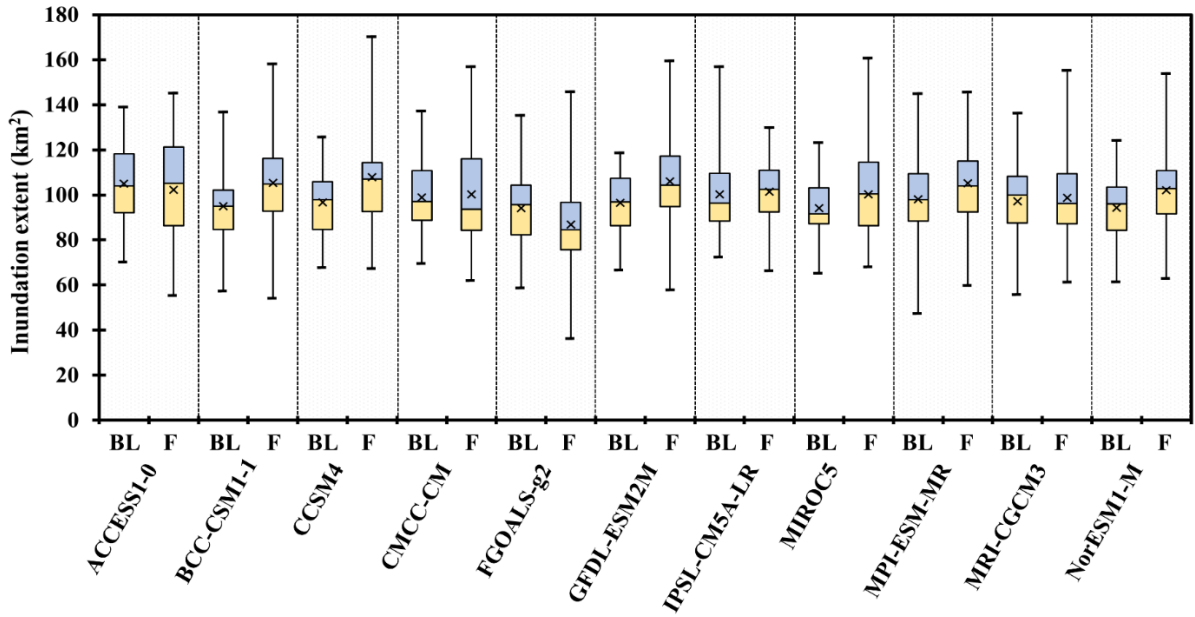
Figure 5. Comparison of simulated maximum flood extent with the corresponding FEMA 1% AEP flood map for the Conasauga River Watershed. Background layer source: © OpenStreetMap contributors 2020. Distributed under a Creative Commons BY-SA License.

539

540 **3.4. Change in Flood Regime**

541 In this section, the projected changes in flood regime were calculated using the
542 flooded area from the baseline and future simulations for each ensemble member. Figure
543 6 illustrates the box and whisker plots for each of the 11 dynamically downscaled GCMs.
544 Given the small sample size in each distribution (40 compared to 440 in Figure 2), the
545 whiskers extend the largest/smallest data points with no outlier detection. For 9 out of the
546 11 downscaled climate models, the mean of 40 flood inundation showed an increase in
547 the floodplain area in the future period. In terms of the 75th percentile and maximum, 10
548 out of 11 models showed increase in the floodplain area. The distribution of maximum
549 future inundation of 4 models are found to be statistically different than their baseline
550 distributions at a 5% significance level. Note that the spread in the future period is
551 generally larger than the spread in the baseline period, suggesting an increase in the
552 hydrologic variability in the future period. Also, while the results from different models
553 were generally consistent, some inter-model differences were noted, which highlight the
554 need of a multi-model framework to capture the uncertainty in the future climate
555 projections. The multi-model approach provides a range of possible flood inundation
556 extents, which is critical for floodplain management decision making. The potential
557 increase in the floodplain area also demonstrates the importance of incorporating climate
558 change projections in the floodplain management regulations.

559



560

561 Figure 6. A summary of simulated maximum flood inundation extents obtained from the
 562 baseline and future scenarios. The mean flooded area values are shown by × symbols.

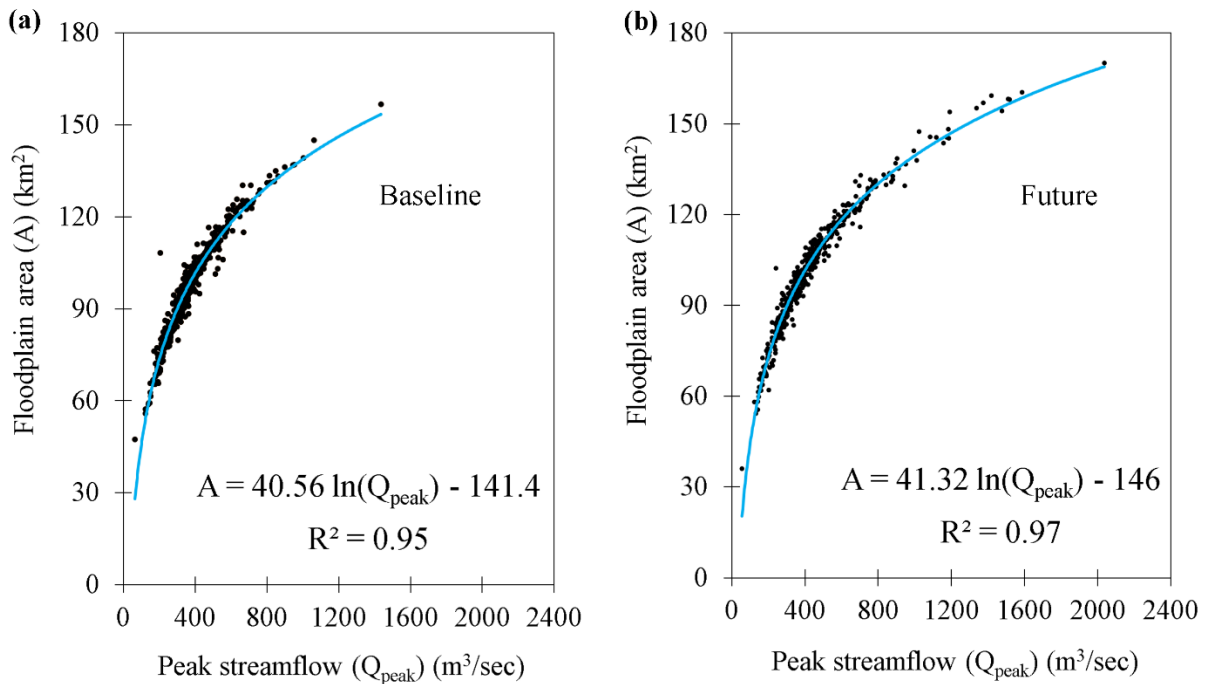
563 Note: The suffix “_BL” represents baseline scenarios and the suffix “_F” represents
 564 future scenarios.

565 3.5. Flood Inundation Frequency Curve and Map

566 Figure 7 shows the relationship between the 440 flooded area values (across 11
 567 downscaled GCMs) and their corresponding peak streamflow at the watershed outlet, for
 568 both the baseline and future periods. Overall, both results (Figure 7a and 7b) exhibit
 569 strong nonlinear relationships with high R^2 values. The results suggest that peak
 570 streamflow is a significant variable controlling the total flooded area, but the variability
 571 of flooded area could not be explained by peak streamflow alone. For instance, in the
 572 baseline period, the peak streamflow values of 423.63 m³/sec and 424.25 m³/sec
 573 correspond to 106.85 km² and 94.89 km² floodplain areas, respectively (Figure 7a).

574 Similarly, in the future period, the peak streamflow values of 433.27 m³/sec and 434.21
575 m³/sec correspond to 110.76 km² and 99.26 km² floodplain areas (Figure 7b).

576



577

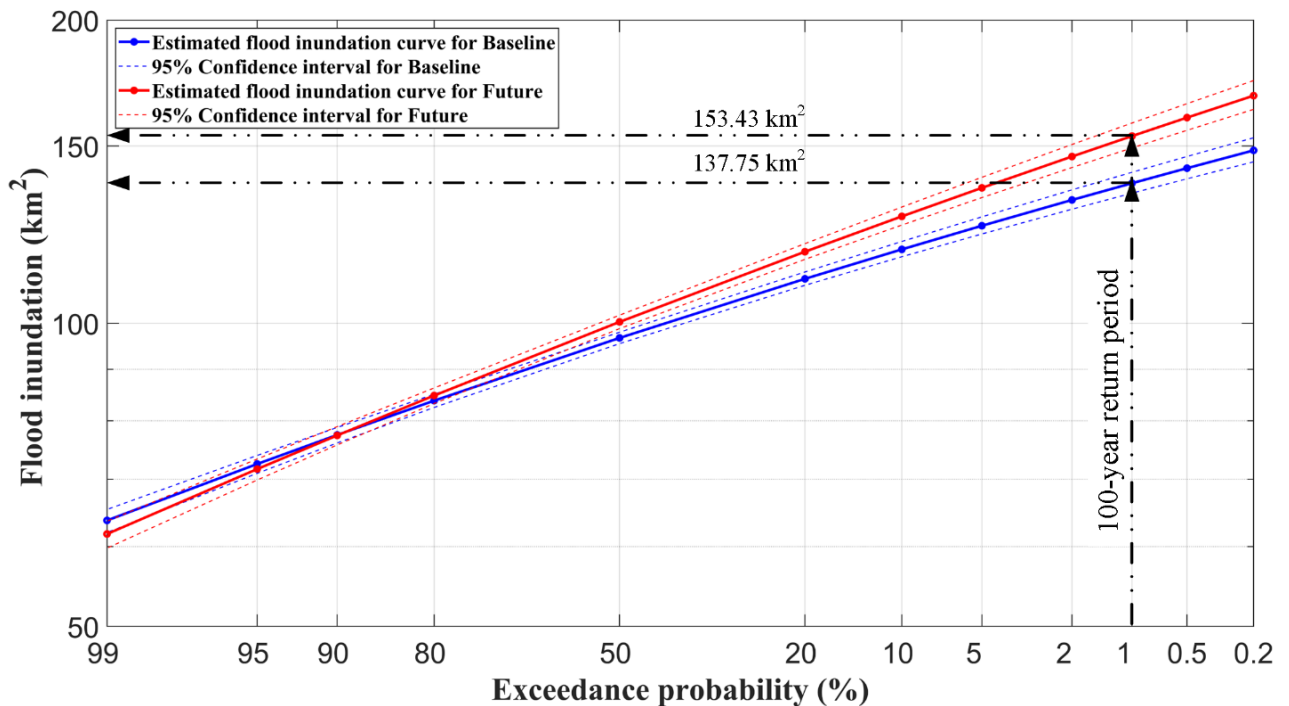
578 Figure 7. Relationship between floodplain areas and peak streamflow values at the
579 watershed outlet for (a) baseline and (b) future scenarios. The blue lines indicate the
580 logarithmic best-fit.

581

582 Figure 8 shows the event-based flood inundation frequency curves and their
583 corresponding 95% confidence intervals in both the baseline and future periods, for
584 which each frequency curve was derived using an ensemble of 440 years of data. The use
585 of long-term data helped reduce the uncertainty and add more confidence in the
586 evaluation of the lower AEP estimates. This type of assessment cannot be achieved using
587 only historic streamflow observations, for which the limited records present a major

588 challenge for lower AEP estimates. For most of the exceedance probabilities, the flooded
 589 areas projected an increase in the inundation areas in the future period when compared to
 590 the baseline period. The 1% AEP flood shows an $\sim 16 \text{ km}^2$ increase in the inundation area
 591 (137.75 km^2 in the baseline period versus 153.43 km^2 in the future period) (Figure 8).
 592 Similar results can be observed in inundation frequency curves developed for other AEPs
 593 (not shown).

594



595

596 Figure 8. A summary of flood inundation frequency curves for the baseline and future
 597 periods.

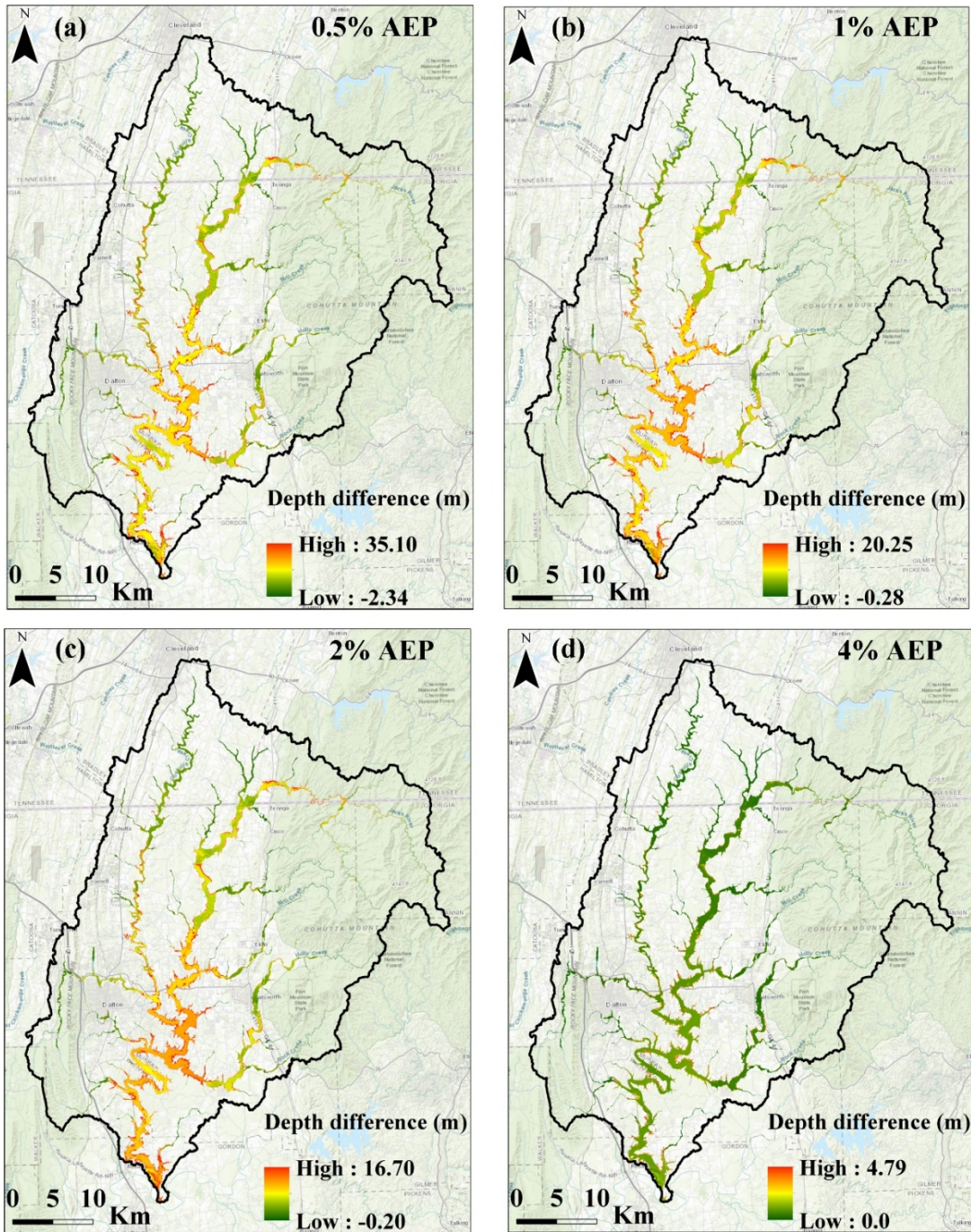
598

599 The grid-based flood depth frequency results at 0.5%, 1%, 2%, and 4% AEP levels
 600 are illustrated in Figure 9. In each panel, the projected change (i.e., future minus baseline)
 601 at each grid is shown. The corresponding histogram across the entire study area is

602 presented in Figure 10. As mentioned in section 2.4, the LP3 distribution was used for
603 frequency analysis. In order to understand the suitability of LP3, we also conducted a
604 comparative analysis to test an alternative log-normal (LN) distribution. By using the
605 Anderson-Darling (Anderson and Darling, 1954) goodness-of-fit test ($\alpha = 0.05$) along
606 with the Akaike Information Criteria (Akaike, 1974), we found no substantial difference
607 between these two distributions (not showed), for the purpose of our application. It is
608 noted, however, that our goal in this study is not to identify the most suitable choice of
609 flood depth distribution. Therefore, other more suitable distributions may exist but this is
610 beyond the scope of this study.

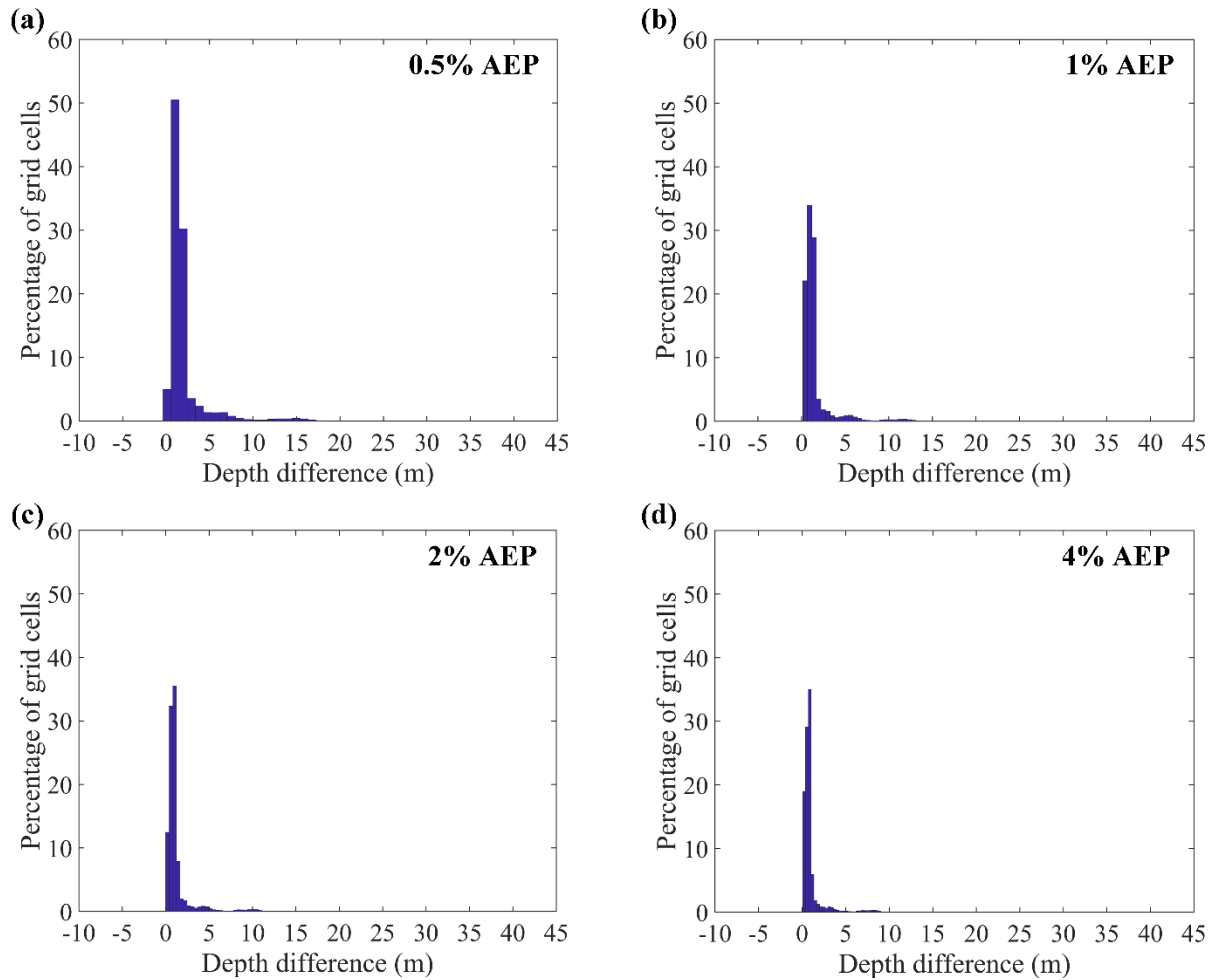
611 Based on the comparisons in Figure 10, it is estimated that the flood depth values at
612 ~80% of grid cells would increase by 0.2 to 1.5 m due to projected changes in climate
613 (Figure 10). For 0.5% and 1% AEP flood depth frequency maps (Figure 9a and 9b), the
614 changes in flood depth were more pronounced in the lower part of the CRW, near the
615 City of Dalton (where there are large population settlements), thereby increasing the
616 likelihood of population exposure to flood risk in the future period. Furthermore, for the
617 1% flood depth frequency map (Figure 9b), the projected increase in flood depths and
618 spatial extent has the potential to extend the flood damage far beyond the FEMA's
619 current base floodplain area. Therefore, these results highlight the need for climate
620 change consideration in the floodplain mapping. The approach presented in this study can
621 provide an alternative floodplain delineation technique, as it can be applied to develop
622 flood depth frequency maps that are reflective of the future climate.

623



624
625
626
627
628
629
630

Figure 9. Projected change (future minus baseline period) in flood depth frequency maps for (a) 0.5%, (b) 1%, (c) 2%, and (d) 4% AEPs. ArcGIS background layer sources: ESRI, HERE, Garmin, Intermap, GEBCO, USGS, Food and Agriculture Organization, National Park Service, Natural Resources Canada, GeoBase, IGN, Kadaster NL, Ordnance Survey, METI, Esri Japan, Esri China, the GIS User Community, and © OpenStreetMap contributors 2020. Distributed under a Creative Commons BY-SA License.



631

632 Figure 10. Histograms for the future changes (2011–2050) in the flood depth relative to
 633 the baseline period (1966–2005) for (a) 0.5%, (b) 1%, (c) 2%, and (d) 4% AEP flood
 634 depth frequency maps.

635

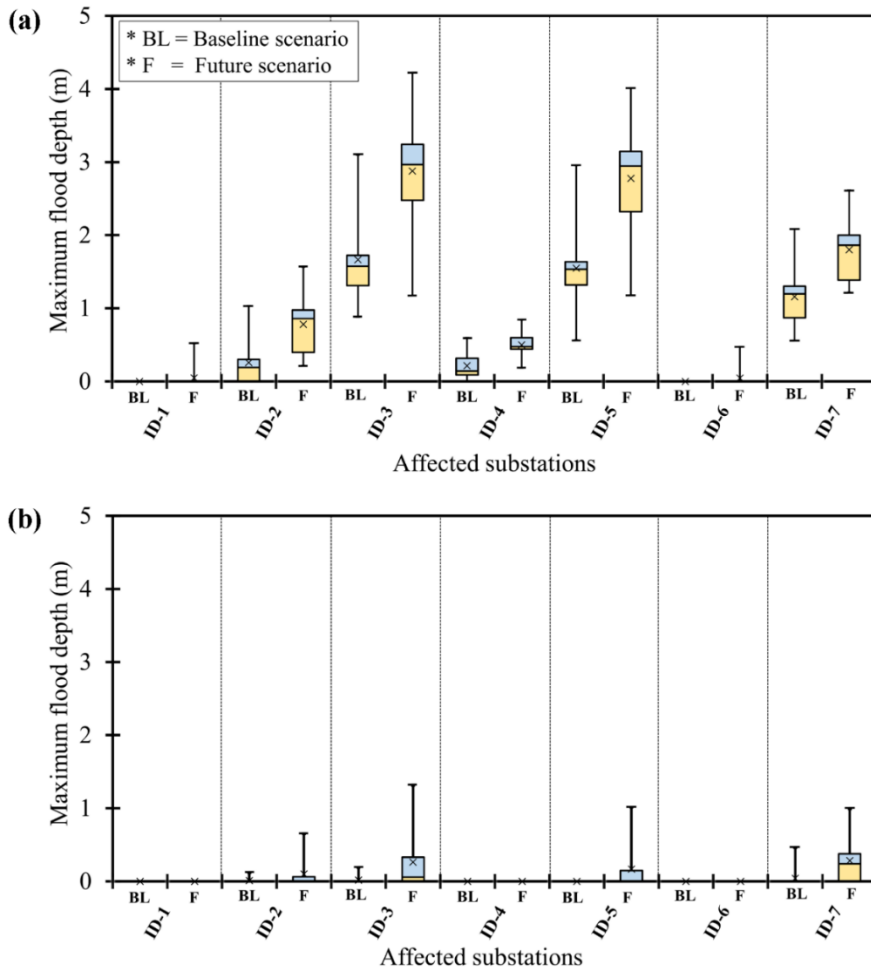
636 3.6. Vulnerability of Electricity Infrastructure

637 Figure 11a shows the box and whisker plot for the distributions of maximum flood
 638 depth values extracted at the substation location across all the baseline and future
 639 simulations, assuming that no flood protection measures were adopted (mitigation
 640 scenario 1). Of the 44 substations, 5 substations could have been affected during the

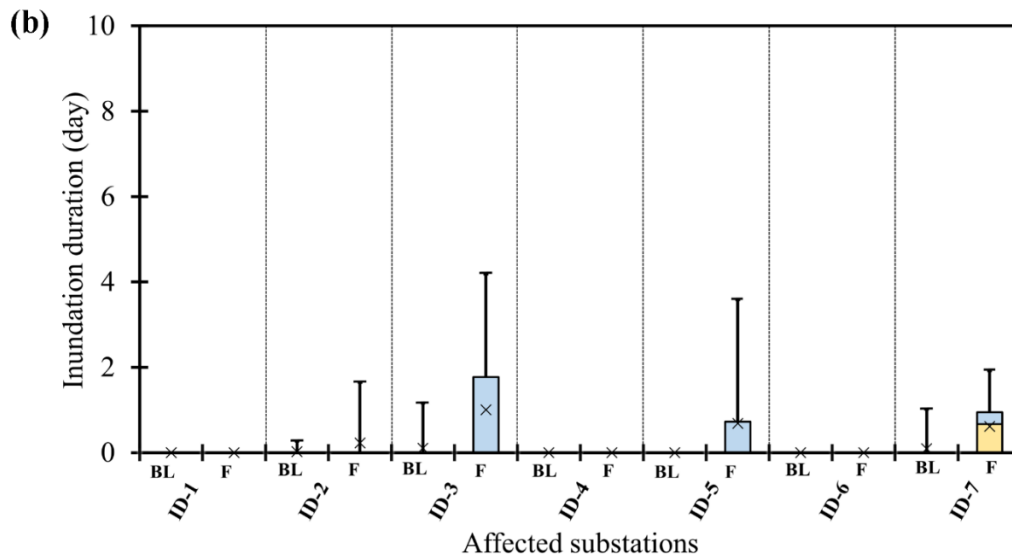
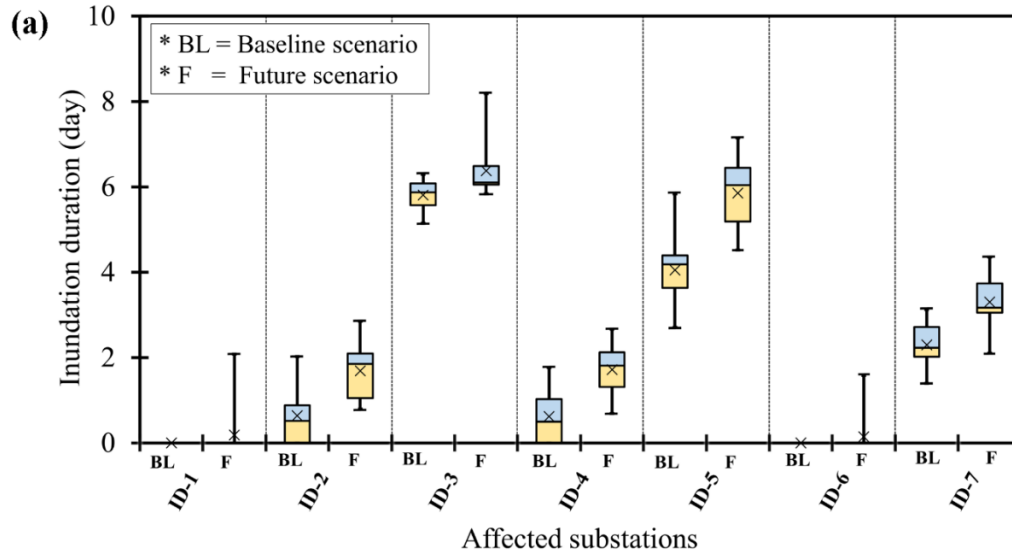
641 baseline period, while 7 substations are projected to be affected during the future period
642 (Figure 11a). Increases are indicated not only for the number of affected substations but
643 also for flood inundation depth values in the projected future climate. Overall, the mean
644 of the ensemble flood depth values shows an ~ 0.6 m increase in the future period (Figure
645 11a). Such an increase in the flood depth magnitude has the potential to exacerbate flood
646 related damage to electrical components, which can inflate the cost of hardening
647 measures such as elevating substations and constructing flood-protective barriers. As
648 expected, when the substations were flood-proofed up to BFE plus ~ 0.91 m (mitigation
649 scenario 2), the number of affected substations is reduced to three and four during the
650 baseline and future periods, respectively (Figure 11b). The locations of substations that
651 were impacted in the baseline period, in both mitigation scenarios, are consistent with the
652 Whitfield County Emergency Management Agency report map (EMA, 2016) that shows
653 the locations of critical facilities vulnerable to the historical flooding.

654 The maximum inundation durations at the affected substations are summarized in
655 Figure 12a (mitigation scenario 1) and Figure 12b (mitigation scenario 2). For both
656 mitigation scenarios and all affected substations, ensemble mean inundation durations
657 exhibited an increase under future climate condition. This increase in inundation duration
658 probably would render substations out of service for longer periods of time by making it
659 difficult to repair damaged substation equipment and restore grid services to customers.
660 The potential hazards and consequences may also extend to critical facilities that are
661 supplied by the affected substations. Similar to results presented in the previous sections,
662 these results demonstrate the need for improving existing flood mitigation measures by
663 incorporating the trends and uncertainties that originate from climate change. The

664 vulnerability analysis approach presented in this study will better equip floodplain
 665 managers to identify the most vulnerable substations and to recommend suitable
 666 adaptation measures, while allocating resources efficiently.



667
 668 Figure 11. A summary of maximum flood depths for substations that were affected in the
 669 baseline and/or future periods (a) without flood protection measures and (b) with flood
 670 protection measures. Note: Affected substations with their corresponding IDs are shown
 671 in Figure 1. There are no negative values in the vertical axis, as the minimum flood depth
 672 value is zero.



673

674 Figure 12. A summary of maximum inundation durations for substations that were
 675 affected in the baseline and/or future periods (a) without flood protection measures and
 676 (b) with flood protection measures. Note: Affected substations with their corresponding
 677 IDs are shown in Figure 1. There are no negative values in the vertical axis, as the
 678 minimum inundation duration is zero.

679

680 4. Summary and Conclusion

681 This paper applies an integrated modeling framework to evaluate climate change
682 impacts on flood regime, floodplain protection standards, and electricity infrastructures
683 across the Conasauga River Watershed in the southeastern United States. Building on the
684 ensemble concept used by Gangrade et al. (2019) for PMF-scale inundation modeling
685 (AEP < 10⁻⁴ %), we focused on more frequent extreme streamflow events (i.e., AEP
686 around 1–0.2%) based on 11 downscaled CMIP5 GCMs in this study. Our evaluation is
687 based on a climate-hydrologic-hydraulic modeling framework, which makes use of an
688 eleven member ensemble of downscaled climate simulations. Nine out of eleven
689 ensemble members project an increase in the flood inundation area in the future period.
690 Similarly, at the 1% AEP level, the flood inundation frequency curves indicate ~16 km²
691 increase in floodplain area under the future climate. The comparison between the flood
692 depth frequency maps from the baseline and future simulations indicated that, on average,
693 ~80% of grid cells exhibit a 0.2 to 1.5 m increase in the flood depth values. Without the
694 flood protection measures, of the 44 electric substations inside the watershed, 5 and 7
695 substations could be affected during the baseline and future periods, respectively. Even
696 after flood-proofing, three and four substations could still be affected in the baseline and
697 future periods. The increases in flood depth magnitude and inundation duration at the
698 affected substations in the future period will most likely damage more electrical
699 components, inflate the cost of hardening measures and render substations out of service
700 for a longer period of time.

701 Although future climate conditions are uncertain, our results demonstrate the needs
702 for (1) consideration of climate change in the floodplain management regulations; (2)

703 improvements in the conventional deterministic flood delineation approach through the
704 inclusion of probabilistic or ensemble-based methods, and (3) improvements in the
705 existing flood protection measures for critical electricity infrastructures through enhanced
706 hydro-meteorologic modeling capacities. In particular, rapidly advanced high-
707 performance computing capabilities have enabled the incorporation of computationally
708 intensive 2D hydraulics modeling in the ensemble-based hydroclimate impact
709 assessment. While the computational cost demonstrated in this study may still seem
710 steep, in the current speed of technology advancement, we will soon be able to implement
711 such a computationally intensive assessment for wide applications. The approach
712 presented in this study can be used by floodplain managers to develop flood depth
713 frequency maps and to identify the most vulnerable electric substations.

714 **Author Contribution**

715 *Dullo, Kalyanapu, Kao, Gangrade and Morales-Hernández* developed the concept for the
716 paper, designed the methodology and *Dullo* performed all the simulations required for the
717 study with feedback from all the co-authors. *Sharif, Ghafoor and Morales-Hernández*
718 focused on programming, software development and testing of existing code components.
719 *Ashfaq and Morales-Hernández* provided access to supercomputing machine hours on
720 ORNL's SUMMIT and RHEA computers. The manuscript was edited by *Dullo* with inputs
721 from the co-authors.

722 **Competing Interests**

723 The authors declare that they have no conflict of interest.

724 **Acknowledgments**

725 This study was supported by the US Air Force Numerical Weather Modeling
726 Program. TTD, MBS, AJK, and SG also acknowledge support by the Center of
727 Management, Utilization, and Protection of Water Resources at Tennessee Technological
728 University. Some portion of the project was funded by the UT Battelle Subcontract No:
729 4000164401. The research used resources of the Oak Ridge Leadership Computing
730 Facility at Oak Ridge National Laboratory. Some of the co-authors are employees of UT-
731 Battelle LLC under contract DE-AC05-00OR22725 with the US Department of Energy.
732 Accordingly, the US government retains and the publisher, by accepting the article for
733 publication, acknowledges that the US government retains a nonexclusive, paid-up,
734 irrevocable, worldwide license to publish or reproduce the published form of this
735 manuscript, or allow others to do so, for US government purposes. The input data sets are
736 cited throughout the paper, as appropriate.

737 **Data Availability**

738 The data that support the findings of this study are openly available in figshare
739 repository at the following URL:

740 https://figshare.com/projects/Conasauga_Flood_Modeling_Project/80840.

741 **References**

742 AECOM: The Impact of Climate Change and Population Growth on the National Flood
743 Insurance Program through 2100, available at: [https://www.aecom.com/content/wp-](https://www.aecom.com/content/wp-content/uploads/2016/06/Climate_Change_Report_AECOM_2013-06-11.pdf)
744 [content/uploads/2016/06/Climate_Change_Report_AECOM_2013-06-11.pdf](https://www.aecom.com/content/uploads/2016/06/Climate_Change_Report_AECOM_2013-06-11.pdf) (last
745 access: 12 October 2019), 2013.

746 Alfieri, L., Salamon, P., Bianchi, A., Neal, J., Bates, P., and Feyen, L.: Advances in Pan-
747 European Flood Hazard Mapping, *Hydrol. Process.*, 28(13), 4067–4077,
748 doi:10.1002/hyp.9947, 2014.

749 Alfieri, L., Burek, P., Feyen, L., and Forzieri, G.: Global Warming Increases the
750 Frequency of River Floods in Europe, *Hydrol. Earth Syst. Sci.*, 19, 2247–2260,
751 doi:10.5194/hess-19-2247-2015, 2015a.

752 Alfieri, L., Feyen, L., Dottori, F., and Bianchi, A.: Ensemble Flood Risk Assessment in
753 Europe Under High End Climate Scenarios, *Global Environ. Chang.*, 35, 199–212,
754 doi:10.1016/j.gloenvcha.2015.09.004, 2015b.

755 Alfieri, L., Bisselink, B., Dottori, F., Naumann, G., de Roo, A., Salamon, P., Wyser, K.,
756 and Feyen, L.: Global Projections of River Flood Risk in a Warmer World, *Earth’s*
757 *Future*, 5, 171–182, doi:10.1002/2016EF000485, 2017.

758 Alfieri, L., Dottori, F., Betts, R., Salamon, P., and Feyen, L.: Multi-Model Projections of
759 River Flood Risk in Europe under Global Warming, *Climate*, 6(6),
760 doi:10.3390/cli6010006, 2018.

761 Allen-Dumas, M. R., Binita, K. C., and Cunliff, C. I.: Extreme Weather and Climate
762 Vulnerabilities of the Electric Grid: A Summary of Environmental Sensitivity
763 Quantification Methods, ORNL/TM-2019/1252, Oak Ridge National Laboratory,
764 available at: [https://www.energy.gov/sites/prod/files/2019/09/f67/
765 Oak%20Ridge%20National%20Laboratory%20EIS%20Response.pdf](https://www.energy.gov/sites/prod/files/2019/09/f67/Oak%20Ridge%20National%20Laboratory%20EIS%20Response.pdf) (last access: 17
766 December 2019), 2019.

767 Anderson, T. W., and Darling, D. A. Asymptotic theory of certain ‘goodness-of-fit’
768 criteria based on stochastic processes, *Ann. Math. Stat.*, 23, 193-212, 1952. URL:
769 <https://www.jstor.org/stable/2236446>

770 Archuleta, C.-A. M., Constance, E. W., Arundel, S. T., Lowe, A. J., Mantey, K. S., and
771 Phillips, L. A.: The National Map Seamless Digital Elevation Model Specifications,
772 US Geological Survey Techniques and Methods 11-B9, doi:10.3133/tm11B9,
773 available at: <https://pubs.er.usgs.gov/publication/tm11B9> (last access: 31 December
774 2019), 2017.

775 Arnell, N. W. and Gosling, S. N.: The Impacts of Climate Change on River Flood Risk at
776 the Global Scale, *Clim. Change*, 134, 387–401, doi:10.1007/s10584-014-1084-5,
777 2014.

778 Ashfaq, M., Bowling, L. C., Cherkauer, K., Pal, J. S., and Diffenbaugh, N. S.: Influence
779 of Climate Model Biases and Daily-scale Temperature and Precipitation Events on
780 Hydrological Impacts Assessment: A Case Study of the United States, *J. Geophys.*
781 *Res.*, 115, D14116, doi:10.1029/2009JD012965, 2010.

782 Ashfaq, M., Ghosh, S., Kao, S.-C., Bowling, L. C., Mote, P., Touma, D., Rauscher, S. A.,
783 and Diffenbaugh, N. S.: Near-term Acceleration of Hydroclimatic Change in the
784 Western U.S., *J. Geophys. Res.*, 118, 10,676–10, 693, doi:10.1002/jgrd.50816, 2013.

785 Ashfaq, M., Rastogi, D., Mei, R., Kao, S.-C., Gangrade, S., Naz, B. S., and Touma, D.:
786 High-resolution Ensemble Projections of Near-term Regional Climate over the
787 Continental United States. *J. Geophys. Res.*, 121, 9943–9963,
788 doi:10.1002/2016JD025285, 2016.

789 Baechler, M. C., Gilbride, T. L., Cole, P. C., Hefty, M. G., and Ruiz, K.: Building
790 America Best Practices Series, Volume 7.3, High-Performance Home Technologies:
791 Guide to Determining Climate Regions by County, Pacific Northwest National
792 Laboratory, US Department of Energy under Contract DE-AC05-76RLO 1830,
793 PNNL-17211 Rev. 3, available at:
794 https://www.energy.gov/sites/prod/files/2015/10/f27/ba_climate_region_guide_7.3.pdf
795 [f](#) (last access: 27 September 2020), 2015.

796 Bhuyian, Md. N. M., Kalyanapu, A. J., and Nardi, F.: Approach to Digital Elevation
797 Model Correction by Improving Channel Conveyance, *J. Hydrol. Eng.*, 20(5),
798 doi:10.1061/(ASCE)HE.1943-5584.0001020, 2014.

799 Bhuyian, Md. N. M., Dullo, T. T., Kalyanapu, A. J., Gangrade, S., and Kao, S.-C.:
800 Application of Geomorphic Correlations for River Bathymetry Correction in Two-
801 dimensional Hydrodynamic Modeling for Long-term Flood Risk Evaluation, World
802 Environmental and Water Resources Congress, Pittsburgh, Pennsylvania, USA, 19-23
803 May 2019, 2019.

804 Birhanu, D., Kim, H., Jang, C., and Park, S.: Flood Risk and Vulnerability of Addis
805 Ababa City Due to Climate Change and Urbanization, *Procedia Engineer.*, 154, 696–
806 702, doi:10.1016/j.proeng.2016.07.571, 2016.

807 Blessing, R., Sebastian, A., and Brody, S. D.: Flood Risk Delineation in the United
808 States: How Much Loss Are We Capturing?, *Nat. Hazards Rev.*, 18(3), 04017002-(1-
809 10), doi:10.1061/(ASCE)NH.1527-6996.0000242, 2017.

810 Bollinger, L. A. and Dijkema, G. P. J.: Evaluating Infrastructure Resilience to Extreme
811 Weather – the Case of the Dutch Electricity Transmission Network, *EJTIR*, 16(1),
812 214–239, doi:10.18757/ejtir.2016.16.1.3122, 2016.

813 Bragatto, T., Cresta, M., Cortesi, F., Gatta, F. M., Geri, A., Maccioni, M., and Paulucci,
814 M.: Assessment and Possible Solution to Increase Resilience: Flooding Threats in
815 Terni Distribution Grid, *Energies*, 12(4), 744, doi:10.3390/en12040744, 2019.

816 Brunner, G. W., Warner, J. C., Wolfe, B. C., Piper, S. S., and Marston, L.: Hydrologic
817 Engineering Center – River Analysis System (HEC-RAS) Applications Guide 2016,
818 Version 5.0, US Army Corps of Engineers, CA, available at:
819 <https://www.hec.usace.army.mil/software/hec-ras/documentation/HEC->
820 [RAS%205.0%20Applications%20Guide.pdf](https://www.hec.usace.army.mil/software/hec-ras/documentation/HEC-RAS%205.0%20Applications%20Guide.pdf) (last access: 27 December 2019), 2016.

821 Burkey, J.: Log-Pearson Flood Flow Frequency using USGS 17B, available at:
822 <https://www.mathworks.com/matlabcentral/fileexchange/22628-log-pearson-flood->
823 [flow-frequency-using-usgs-17b](https://www.mathworks.com/matlabcentral/fileexchange/22628-log-pearson-flood-flow-frequency-using-usgs-17b) (last access: 23 December 2019), 2009.

824 Chandramowli, S. N. and Felder, F. A.: Impact of Climate Change on Electricity Systems
825 and Markets – A Review of Models and Forecasts, *Sustain. Energy Technol. Assess.*,
826 5, 62–74, doi:10.1016/j.seta.2013.11.003, 2014.

827 Ciscar, J. C. and Dowling, P.: Integrated Assessment of Climate Impacts and Adaptation
828 in the Energy Sector, *Energy Econ.*, 46, 531–538, doi:10.1016/j.eneco.2014.07.003,
829 2014.

830 Cronin, J., Anandarajah, G., and Dessens, O.: Climate Change Impacts on the Energy
831 System: A Review of Trends and Gaps, *Clim. Change*, 151, 79–93,
832 doi:10.1007/s10584-018-2265-4, 2018.

833 Cook, A. and Merwade, V.: Effect of topographic data, geometric configuration and
834 modeling approach on flood inundation mapping, *J. Hydrol.*, 377(1-2), 131-142,
835 doi:10.1016/j.jhydrol.2009.08.015, 2009.

836 Daly, C., Halbleib, M., Smith, J. I., Gibson, W. P., Doggett, M. K., Taylor, G. H., Curtis,
837 J., and Pasteris, P. P.: Physiographically Sensitive Mapping of Climatological
838 Temperature and Precipitation Across the Conterminous United States, *Int. J.*
839 *Climatol.*, 28(15), 2031–2064, doi:10.1002/joc.1688, 2008.

840 Dey, S., Saksena, S., and Merwade, V.: Assessing the effect of different bathymetric
841 models on hydraulic simulation of rivers in data sparse regions, *J. Hydrol.*, 575, 838-
842 851, doi:10.1016/j.jhydrol.2019.05.085, 2019.

843 Elliott, K. J. and Vose, J. M.: Initial Effects of Prescribed Fire on Quality of Soil Solution
844 and Streamwater in the Southern Appalachian Mountains, *South. J. Appl. For.*, 29(1),
845 5–15, doi:10.1093/sjaf/29.1.5, 2005.

846 Elsner, M. M., Cuo, L., Voisin, N., Deems, J. S., Hamlet, A. F., Vano, J. A., Mickelson,
847 K. E. B., Lee, S.-Y., and Lettenmaier, D. P.: Implications of 21st Century Climate
848 Change for the Hydrology of Washington State, *Climatic Change*, 102(1–2), 225–
849 260, doi:10.1007/s10584-010-9855-0, 2010.

850 EMA (Emergency Management Agency): Whitfield County Hazard Mitigation Plan
851 2016, Including the Cities of Dalton, Tunnel Hill, and Varnell, and the Town of
852 Cohutta, Whitfield County Emergency Management Agency, available at:
853 <https://www.whitfieldcountyga.com/ema/WhitfieldHMPDraft52616.pdf> (last access:
854 29 March 2020), 2016.

855 England Jr., J. F., Cohn, T. A., Faber, B. A., Stedinger, J. R., Thomas Jr., W. O.,
856 Veilleux, A. G., Kiang, J. E., and Mason Jr., R. R.: Guidelines for Determining Flood
857 Flow Frequency—Bulletin 17C, Techniques and Methods 4-B5, US Geological
858 Survey, <https://doi.org/10.3133/tm4B5>, 2019.

859 Farber-DeAnda, M., Cleaver, M., Lewandowski, C., and Young, K.: Hardening and
860 Resiliency: US Energy Industry Response to Recent Hurricanes Seasons, Office of
861 Electricity Delivery and Energy Reliability, US Department of Energy, available at:
862 <https://www.oe.netl.doe.gov/docs/HR-Report-final-081710.pdf> (last access: 17
863 December 2019), 2010.

864 FEMA (Federal Emergency Management Agency): National Flood Insurance Program:
865 Program Description, Federal Emergency Management Agency, available at:
866 [https://www.fema.gov/media-library-data/20130726-1447-20490-
867 2156/nfipdescrip_1_.pdf](https://www.fema.gov/media-library-data/20130726-1447-20490-2156/nfipdescrip_1_.pdf) (last access: 22 January 2018), 2002.

868 FEMA (Federal Emergency Management Agency): Emergency Power Systems for
869 Critical Facilities: A Best Practices Approach to Improving Reliability, FEMA P-
870 1019, Applied Technology Council, Redwood City, CA, available at:
871 <https://www.fema.gov/media-library/assets/documents/101996> (last access: 17
872 December 2019), 2014.

873 FEMA (Federal Emergency Management Agency): FEMA Flood Map Service Center,
874 available at: <https://msc.fema.gov/portal/availabilitySearch?#searchresultsanchor>
875 (last access: 28 December 2019), 2019.

876 FIS (Flood Insurance Study): Flood Insurance Study: Whitfield County, Georgia and
877 Incorporated Areas, Flood Insurance Study Number: 13313CV000A, Federal

878 Emergency Management Agency, available at:
879 <http://www.georgiadfirm.com/pdf/panels/13313CV000A.pdf> (last access: 25
880 December 2019), 2007.

881 FIS (Flood Insurance Study): Flood Insurance Study: Murray County, Georgia and
882 Incorporated Areas, Flood Insurance Study Number: 13213CV000A, Federal
883 Emergency Management Agency, available at:
884 <http://www.georgiadfirm.com/pdf/panels/13213CV000A.pdf> (last access: 27
885 December 2019), 2010.

886 Forzieri, G., Bianchi, A., e Silva, F. B., Herrera, M. A. M., Leblois, A., Lavallo, C.,
887 Aerts, J. C. J. H., and Feyen, L.: Escalating Impacts of Climate Extremes on Critical
888 Infrastructures in Europe, *Glob. Environ. Change*, 48, 97–107,
889 doi:10.1016/j.gloenvcha.2017.11.007, 2018.

890 Fu, G., Wilkinson, S., Dawson, R. J., Fowler, H. J., Kilsby, C., Panteli, M., and
891 Mancarella, P.: Integrated Approach to Assess the Resilience of Future Electricity
892 Infrastructure Networks to Climate Hazards, *IEEE Syst. J.*, 12(4), 3169–3180,
893 doi:10.1109/JSYST.2017.2700791, 2017.

894 Galloway, G. E., Baecher, G. B., Plasencia, D., Coulton, K. G., Louthain, J., Bagha, M.,
895 and Levy, A. R.: Assessing the Adequacy of the National Flood Insurance Program’s
896 1 Percent Flood Standard, Water Policy Collaborative, University of Maryland,
897 available at: <https://www.fema.gov/media-library/assets/documents/9594> (last access:
898 17 December 2019), 2006.

899 Gangrade, S., Kao, S.-C., Naz, B. S., Rastogi, D., Ashfaq, M., Singh, N., and Preston, B.
900 L.: Sensitivity of Probable Maximum Flood in a Changing Environment, *Water*
901 *Resour. Res.*, 54(6), 3913–3936, doi:10.1029/2017WR021987, 2018.

902 Gangrade, S., Kao, S.-C., Dullo, T. T., Kalyanapu, A. J., and Preston, B. L.: Ensemble-
903 based Flood Vulnerability Assessment for Probable Maximum Flood in a Changing
904 Environment, *J. Hydrol.*, 576, 342–355, doi:10.1016/j.jhydrol.2019.06.027, 2019.

905 Gangrade, S., Kao, S.-C., and McManamay, R. A.: Multi-model Hydroclimate
906 Projections for the Alabama-Coosa-Tallapoosa River Basin in the Southeastern
907 United States, *Sci. Rep.*, 10, 2870, doi:10.1038/s41598-020-59806-6, 2020.

908 Gilstrap, M., Amin, S., and DeCorla-Souza, K.: United States Electricity Industry Primer,
909 DOE/OE-0017, Office of Electricity Delivery and Energy Reliability, US Department
910 of Energy, Washington DC, available at:
911 [https://www.energy.gov/sites/prod/files/2015/12/f28/united-states-electricity-
912 industry-primer.pdf](https://www.energy.gov/sites/prod/files/2015/12/f28/united-states-electricity-
912 industry-primer.pdf) (last access: 17 December 2019), 2015.

913 Giorgi, F., Coppola, E., Solmon, F., Mariotti, L., Sylla, M. B., Bi, X., Elguindi, N., Diro,
914 G. T., Nair, V., Giuliani, G., Turuncoglu, U. U., Cozzini, S., Güttler, I., O’Brien, T.
915 A., Tawfik, A. B., Shalaby, A., Zakey, A. S., Steiner, A. L., Stordal, F., Sloan, L. C.,
916 and Brankovic, C.: RegCM4: model description and preliminary tests over multiple
917 CORDEX domains, *Climate Res.*, 52, 7–29, doi:10.3354/cr01018, 2012.

918 HCFCD (Harris County Flood Control District): Hurricane Harvey – Storm and Flood
919 Information, available at: [https://www.hcfd.org/Portals/62/Harvey/immediate-flood-
920 report-final-hurricane-harvey-2017.pdf](https://www.hcfd.org/Portals/62/Harvey/immediate-flood-
920 report-final-hurricane-harvey-2017.pdf) (last access: 16 December 2019), 2018.

921 HIFLD (Homeland Infrastructure Foundation-Level Data): Homeland Infrastructure
922 Foundation-Level Data, Electric Substations, US Department of Homeland Security,
923 available at: [https://hifld-geoplatform.opendata.arcgis.com/datasets/electric-
925 substations](https://hifld-geoplatform.opendata.arcgis.com/datasets/electric-
924 substations) (last access: 20 December 2019), 2019.

925 Hirabayashi, Y., Mahendran, R., Koirala, S., Konoshima, L., Yamazaki, D., Watanabe,
926 S., Kim, H., and Kanae, S.: Global Flood Risk under Climate Change, *Nature Clim.*
927 *Chang.*, 3, 816–821, doi:10.1038/NCLIMATE1911, 2013.

928 Hou, Z., Ren, H., Sun, N., Wigmosta, M. S., Liu, Y., Leung, L. R., Yan, H., Skaggs, R.,
929 and Coleman, A.: Incorporating Climate Nonstationarity and Snowmelt Processes in
930 Intensity–Duration–Frequency Analyses with Case Studies in Mountainous Areas, *J.*
931 *Hydrometeorol.*, 20(12), 2331–2346, doi:10.1175/JHM-D-19-0055.1, 2019.

932 Ivey, G. and Evans, K.: Conasauga River Alliance Business Plan: Conasauga River
933 Watershed Ecosystem Project, available at: [https://www.fs.fed.us/
935 largewatershedprojects/businessplans/](https://www.fs.fed.us/
934 largewatershedprojects/businessplans/) (last access: 22 December 2019), 2000.

935 Kalyanapu, A. J., Burian, S. J., and McPherson, T. N.: Effect of Land Use-Based Surface
936 Roughness on Hydrologic Model Output, *Journal of Spatial Hydrology*, 9(2), 51–71,
937 2009.

938 Kalyanapu, A. J., Shankar, S., Pardyjak, E. R., Judi, D. R., and Burian, S. J.: Assessment
939 of GPU Computational Enhancement to a 2D Flood Model, *Environ. Modell. Softw.*,
940 26(8), 1009–1016, doi:10.1016/j.envsoft.2011.02.014, 2011.

941 Kefi, M., Mishra, B. K., Kumar, P., Masago, Y., and Fukushi, K.: Assessment of
942 Tangible Direct Flood Damage Using a Spatial Analysis Approach under the Effects

943 of Climate Change: Case Study in an Urban Watershed in Hanoi, Vietnam, *Int. J.*
944 *Geo-Inf.*, 7, 29, doi:10.3390/ijgi7010029, 2018.

945 Kollat, J. B., Kasprzyk, J. R., Thomas Jr., W. O., Miller, A. C., and Divoky, D.:
946 Estimating the Impacts of Climate Change and Population Growth on Flood
947 Discharges in the United States, *J. Water Resour. Plann. Manage.*, 138(5), 442–452,
948 doi:10.1061/(ASCE)WR.1943-5452.0000233, 2012.

949 Langerwisch, F., Rost, S., Gerten, D., Poulter, B., Rammig, A., and Cramer, W.: Potential
950 Effects of Climate Change on Inundation Patterns in the Amazon Basin, *Hydrol.*
951 *Earth Syst. Sci.*, 17, 2247–2262, doi:10.5194/hess-17-2247-2013, 2013.

952 Li, H., Sun, J., Zhang, H., Zhang, J., Jung, K., Kim, J., Xuan, Y., Wang, X., and Li, F.:
953 What Large Sample Size Is Sufficient for Hydrologic Frequency Analysis? – A
954 Rational Argument for a 30-Year Hydrologic Sample Size in Water Resources
955 Management, *Water*, 10, 430, doi:10.3390/w10040430, 2018.

956 Marshall, R., Ghafoor, S., Rogers, M., Kalyanapu, A., and Dullo, T. T.: Performance
957 Evaluation and Enhancements of a Flood Simulator Application for Heterogeneous
958 HPC Environments, *Int. J. Network Comput.*, 8(2), 387–407, 2018.

959 McCuen, R. H.: *Hydrologic Analysis and Design*, Third Edition, Pearson-Prentice Hall,
960 Upper Saddle River, New Jersey, 2005.

961 Mikellidou, C. V., Shakou, L. M., Boustras, G., and Dimopoulos, C.: Energy Critical
962 Infrastructures at Risk from Climate Change: A State of the Art Review, *Saf. Sci.*,
963 110, 110–120, doi:10.1016/j.ssci.2017.12.022, 2018.

964 Milly, P. C. D., Wetherald, R. T., Dunne, K. A., and Delworth, T. L.: Increasing Risk of
965 Great Floods in a Changing Climate, *Nature*, 415(6871), 514–517,
966 doi:10.1038/415514a, 2002.

967 Mora, C., Spirandelli, D., Franklin, E. C., Lynham, J., Kantar, M. B., Miles, W., Smith,
968 C. Z., Freel, K., Moy, J., Louis, L. V., Barba, E. W., Bettinger, K., Frazier, A. G.,
969 Colburn IX, J. F., Hanasaki, N., Hawkins, E., Hirabayashi, Y., Knorr, W., Little, C.
970 M., Emanuel, K., Sheffield, J., Patz, J. A., and Hunter, C. L.: Broad Threat to
971 Humanity from Cumulative Climate Hazards Intensified by Greenhouse Gas
972 Emissions, *Nature Clim. Chang.*, 8, 1062–1071, doi:10.1038/s41558-018-0315-6,
973 2018.

974 Morales-Hernández, M., Sharif, M. B., Gangrade, S., Dullo, T. T., Kao, S.-C.,
975 Kalyanapu, A., Ghafoor, S. K., Evans, K. J., Madadi-Kandjani, E., and Hodges, B. R.:
976 High Performance Computing in Water Resources Hydrodynamics, *Journal of*
977 *Hydroinformatics*, in press, 2020.

978 Morales-Hernández, M., Sharif, Md. B., Kalyanapu, A., Ghafoor, S. K., Dullo, T.T.,
979 Gangrade, S., Kao, S.-C., Norman, M. R., and Evans, K. J.: TRITON: A Multi-GPU
980 Open Source 2D Hydrodynamic Flood, *Environmental Modelling & Software*, in
981 press, 2021.

982 MRLC (Multi-Resolution Land Characteristics Consortium): National Land Cover
983 Database (NLCD), available at: [https://www.mrlc.gov/data/nlcd-2011-land-cover-](https://www.mrlc.gov/data/nlcd-2011-land-cover-conus-0)
984 [conus-0](https://www.mrlc.gov/data/nlcd-2011-land-cover-conus-0) (last access: 5 May 2020), 2011.

985 NERC (North American Electric Reliability Corporation): Hurricane Harvey Event
986 Analysis Report, North American Electric Reliability Corporation, Atlanta, GA,

987 available at: [https://www.nerc.com/pa/rrm/ea/Hurricane_Harvey_EAR_DL/](https://www.nerc.com/pa/rrm/ea/Hurricane_Harvey_EAR_DL/NERC_Hurricane_Harvey_EAR_20180309.pdf)
988 [NERC Hurricane Harvey EAR 20180309.pdf](https://www.nerc.com/pa/rrm/ea/Hurricane_Harvey_EAR_20180309.pdf) (last access: 17 December 2019),
989 2018.

990 Ntelekos, A. A., Oppenheimer, M., Smith, J. A., and Miller, A. J.: Urbanization, Climate
991 Change and Flood Policy in the United States, *Clim. Chang.*, 103, 597–616,
992 doi:10.1007/s10584-009-9789-6, 2010.

993 Nyaupane, N., Thakur, B., Kalra, A., and Ahmad, S.: Evaluating Future Flood Scenarios
994 Using CMIP5 Climate Projections, *Water*, 10, 1866, doi:10.3390/w10121866, 2018.

995 Olsen, J. R.: Climate Change and Floodplain Management in the United States, *Clim.*
996 *Change*, 76, 407–426, doi:10.1007/s10584-005-9020-3, 2006.

997 Pachauri, R. K. and Meyer, L. A.: Intergovernmental Panel on Climate Change (IPCC):
998 Climate Change 2014: Synthesis Report, in Proceedings of Contribution of Working
999 Groups I, II and III to the Fifth Assessment Report of the Intergovernmental Panel on
1000 Climate Change, Geneva, Switzerland, available at:
1001 https://www.ipcc.ch/site/assets/uploads/2018/05/SYR_AR5_FINAL_full_wcover.pdf
1002 (last access: 16 December 2019), 2014.

1003 Pant, R., Thacker, S., Hall, J. W., Alderson, D., and Barr, S.: Critical Infrastructure
1004 Impact Assessment Due to Flood Exposure, *J. Flood Risk Manag.*, 11, 22–33,
1005 doi:10.1111/jfr3.12288, 2017.

1006 Pielke Jr., R. A. and Downton, M. W.: Precipitation and Damaging Floods: Trends in the
1007 United States, 1932–97, *J. Climate*, 13(20), 3625–3637, doi:10.1175/1520-
1008 0442(2000)013<3625:PADFTI>2.0.CO;2, 2000.

1009 Pielke Jr., R. A., Downton, M. W., and Barnard Miller, J. Z.: Flood Damage in the United
1010 States, 1926-2000: A reanalysis of National Weather Service Estimates, National
1011 Center for Atmospheric Research, Boulder, CO, available at:
1012 <https://sciencepolicy.colorado.edu/flooddamagedata/flooddamagedata.pdf> (last
1013 access: 16 December 2019), 2002.

1014 Pralle, S.: Drawing Lines: FEMA and the Politics of Mapping Flood Zones, *Clim.*
1015 *Chang.*, 152, 227–237, doi:10.1007/s10584-018-2287-y, 2019.

1016 Reed, D. A., Kapur, K. C., and Christie, R. D.: Methodology for Assessing the Resilience
1017 of Networked Infrastructure, *IEEE Syst. J.*, 3(2), 174–180,
1018 doi:10.1109/JSYST.2009.2017396, 2009.

1019 Saksena, S., Dey, S., Merwade, V., & Singhofen, P. J. (2020). A computationally
1020 efficient and physically based approach for urban flood modeling using a flexible
1021 spatiotemporal structure. *Water Resources Research*, 56, e2019WR025769.
1022 <https://doi.org/10.1029/2019WR025769>

1023 Storck, P., Bowling, L., Wetherbee, P., and Lettenmaier, D.: Application of a GIS-Based
1024 Distributed Hydrology Model for Prediction of Forest Harvest Effects on Peak
1025 Stream Flow in the Pacific Northwest, *Hydrol. Process.*, 12(6), 889–904,
1026 doi:10.1002/(SICI)1099-1085(199805)12:6<889::AID-HYP661>3.0.CO;2-P, 1998.

1027 Strauss, B. and Ziemiński, R.: Sea Level Rise Threats to Energy Infrastructure: A
1028 Surging Seas Brief Report by Climate Central, Climate Central, Washington, DC,
1029 available at: <http://slr.s3.amazonaws.com/SLR-Threats-to-Energy-Infrastructure.pdf>
1030 (last access: 17 December 2019), 2012.

1031 Tan, A.: Sandy and Its Impacts: Chapter 1, NYC Special Initiative for Rebuilding and
1032 Resiliency, NYC Resources, NY, available at:
1033 http://www.nyc.gov/html/sirr/downloads/pdf/final_report/Ch_1_SandyImpacts_FINAL_singles.pdf
1034 (last access: 17 December 2019), 2013.

1035 Thornton, P. E., Running, S. W., and White, M. A.: Generating surfaces of daily
1036 meteorological variables over large regions of complex terrain, J. Hydrol., 190, 214–
1037 251, doi:10.1016/S0022-1694(96)03128-9, 1997.

1038 UNISDR (United Nations Office for Disaster Risk Reduction): Making Development
1039 Sustainable: The Future of Disaster Risk Management, Global Assessment Report on
1040 Disaster Risk Reduction, Geneva, Switzerland, available at:
1041 [https://www.preventionweb.net/english/hyogo/gar/2015/en/gar-
1042 pdf/GAR2015_EN.pdf](https://www.preventionweb.net/english/hyogo/gar/2015/en/gar-pdf/GAR2015_EN.pdf) (last access: 16 December 2019), 2015.

1043 USACE (US Army Corps of Engineers): Master Water Control Manual: Alabama-Coosa-
1044 Tallapoosa (ACT) River Basin, Alabama, Georgia, US Army Corps of Engineers,
1045 available at: [https://www.sam.usace.army.mil/Portals/46/docs/
1046 planning_environmental/act/docs/New/ACT%20Master%20Manual_March%202013.pd
1047 f](https://www.sam.usace.army.mil/Portals/46/docs/planning_environmental/act/docs/New/ACT%20Master%20Manual_March%202013.pdf) (last access: 22 December 2019), 2013.

1048 USGS (US Geological Survey): Guidelines for Determining Flood Flow Frequency,
1049 Bulletin #17B of the Hydrology Subcommittee, Interagency Advisory Committee on
1050 Water Data, US Geological Survey, Reston, VA, 1982.

1051 Vale, M.: Securing the US Electrical Grid, Center for the Study of the Presidency and
1052 Congress (CSPC), Washington DC, available at: [https://protectourpower.org/
1053 resources/cspc-2014.pdf](https://protectourpower.org/resources/cspc-2014.pdf) (last access: 14 March 2017), 2014.

1054 Wigmosta, M. S., Vail, L. W., and Lettenmaier, D. P.: A Distributed Hydrology-
1055 Vegetation Model for Complex Terrain, *Water Resour. Res.*, 30(6), 1665–1679,
1056 doi:10.1029/94WR00436, 1994.

1057 Wigmosta, M. S., Nijssen, B., Storck, P., and Lettenmaier, D. P.: The Distributed
1058 Hydrology Soil Vegetation Model, in *Mathematical Models of Small Watershed
1059 Hydrology and Applications*, V. P. Singh, D. K. Frevert, eds., *Wat. Resour.
1060 Publications*, Littleton, CO, 2002.

1061 Wilbanks, T. J., Bhatt, V., Bilello, D., Bull, S., Ekmann, J., Horak, W., Huang, Y. J.,
1062 Levine, M. D., Sale, M. J., Schmalzer, D., and Scott, M. J.: Effects of Climate
1063 Change on Energy Production and Use in the United States, *US Climate Change
1064 Science Program Synthesis and Assessment Product 4.5*, available at:
1065 <https://digitalcommons.unl.edu/cgi/viewcontent.cgi?article=1005&context=usdoepub>
1066 (last access: 17 December 2019), 2008.

1067 Wing, O. E. J., Bates, P. D., Sampson, C. C., Smith, A. M., Johnson, K. A., and Erickson,
1068 T. A.: Validation of a 30 m Resolution Flood Hazard Model of the Conterminous
1069 United States, *Water Resour. Res.*, 53, 7968–7986, doi:10.1002/2017WR020917,
1070 2017.

1071 Wing, O. E. J., Bates, P. D., Smith, A. M., Sampson, C. C., Johnson, K. A., Fargione, J.,
1072 and Morefield, P.: Estimates of Present and Future Flood Risk in the Conterminous
1073 United States, *Environ. Res. Lett.*, 13(3), 034023, doi:10.1088/1748-9326/aac65,
1074 2018.

1075 Winkler, J., Duenas-Osorio, L., Stein, R., and Subramanian, D.: Performance Assessment
1076 of Topologically Diverse Power Systems Subjected to Hurricane Events, *Reliability*

1077 Engineering and System Safety, 95(4), 323–336, doi:10.1016/j.ress.2009.11.002,
1078 2010.

1079 Winsemius, H. C., Aerts, J. C. J. H., van Beek, L. P. H., Bierkens, M. F. P., Bouwman,
1080 A., Jongman, B., Kwadijk, J. C. J., Ligtoet, W., Lucas, P. L., van Vuuren, D. P., and
1081 Ward, P. J.: Global Drivers of Future River Flood Risk, Nat. Clim. Chang., 6, 381–
1082 385, doi:10.1038/NCLIMATE2893, 2016.

1083 Wobus, C., Gutmann, E., Jones, R., Rissing, M., Mizukami, N., Lorie, M., Mahoney, H.,
1084 Wood, A. W., Mills, D., and Martinich, J.: Climate Change Impacts on Flood Risk
1085 and Asset Damages within Mapped 100-year Floodplains of the Contiguous United
1086 States, Nat. Hazards Earth Syst. Sci., 17, 2199–2211, doi:10.5194/nhess-17-2199-
1087 2017, 2017.

1088 Zamuda, C., Antes, M., Gillespie, C. W., Mosby, A., and Zotter, B.: Climate Change and
1089 the US Energy Sector: Regional Vulnerabilities and Resilience Solutions, Office of
1090 Energy Policy and Systems Analysis, US Department of Energy, available at:
1091 [https://energy.gov/sites/prod/files/2015/10/f27/Regional_Climate_Vulnerabilities_an](https://energy.gov/sites/prod/files/2015/10/f27/Regional_Climate_Vulnerabilities_and_Resilience_Solutions_0.pdf)
1092 [d_Resilience_Solutions_0.pdf](https://energy.gov/sites/prod/files/2015/10/f27/Regional_Climate_Vulnerabilities_and_Resilience_Solutions_0.pdf) (last access: 17 December 2019), 2015.

1093 Zamuda, C. and Lippert, A.: Climate Change and the Electricity Sector: Guide for
1094 Assessing Vulnerabilities and Developing Resilience Solutions to Sea Level Rise,
1095 Office of Energy Policy and Systems Analysis, US Department of Energy, available
1096 at: [https://toolkit.climate.gov/sites/default/files/Climate%20Change%20](https://toolkit.climate.gov/sites/default/files/Climate%20Change%20and%20the%20Electricity%20Sector%20Guide%20for%20Assessing%20Vulnerabilities%20and%20Developing%20Resilience%20Solutions%20to%20Sea%20Level%20Rise%20July%202016.pdf)
1097 [and%20the%20Electricity%20Sector%20Guide%20for%20Assessing%20Vulnerabili](https://toolkit.climate.gov/sites/default/files/Climate%20Change%20and%20the%20Electricity%20Sector%20Guide%20for%20Assessing%20Vulnerabilities%20and%20Developing%20Resilience%20Solutions%20to%20Sea%20Level%20Rise%20July%202016.pdf)
1098 [ties%20and%20Developing%20Resilience%20Solutions%20to%20Sea%20Level%2](https://toolkit.climate.gov/sites/default/files/Climate%20Change%20and%20the%20Electricity%20Sector%20Guide%20for%20Assessing%20Vulnerabilities%20and%20Developing%20Resilience%20Solutions%20to%20Sea%20Level%20Rise%20July%202016.pdf)
1099 [0Rise%20July%202016.pdf](https://toolkit.climate.gov/sites/default/files/Climate%20Change%20and%20the%20Electricity%20Sector%20Guide%20for%20Assessing%20Vulnerabilities%20and%20Developing%20Resilience%20Solutions%20to%20Sea%20Level%20Rise%20July%202016.pdf) (last access: 18 December 2019), 2016.

- 1100 Zhao, G., Gao, H., Naz, B. S., Kao, S.-C., and Voisin, N.: Integrating a Reservoir
1101 Regulation Scheme into a Spatially Distributed Hydrological Model, *Adv. Water*
1102 *Resour.*, 98, 16–31, doi:10.1016/j.advwatres.2016.10.014, 2016.
- 1103 Zheng, X., Maidment, D. R., Tarboton, D. G., Liu, Y. Y., and Passalacqua, P.: GeoFlood:
1104 Large-scale Flood Inundation Mapping Based on High-Resolution Terrain Analysis,
1105 *Water Resour. Res.*, 54, 10,013–10,033, doi:10.1029/2018WR023457, 2018.